I. KINETICS OF THE THERMAL DECOMPOSITION OF NITROGEN DIOXIDE BEHIND SHOCK WAVES

II. KINETICS OF THE FERROUS ION-OXYGEN REACTION IN SULFURIC ACID SOLUTION

Thesis by

Robert Eugene Huffman

In Partial Fulfillment of the Requirements

For the Degree of

Doctor of Philosophy

California Institute of Technology

Pasadena, California

1958

ACKNOWLEDGEMENTS

I would like to express my gratitude to Professor Norman Davidson, who has directed the research presented here. His guidance, enthusiasm, and patience have been greatly appreciated. Professor E. H. Swift has supervised my teaching experience, and his stimulating direction is acknowledged. I would especially like to thank all the people in Professor Davidson's group who preceded me on the shock tube project for the development of procedures and the construction of apparatus.

The Corning Glass Works Foundation and the General Education Board have each contributed fellowships, and their support is gratefully acknowledged. The shock wave research was financially supported by the Office of Naval Research, and the ferrous ion kinetics research was supported by the Atomic Energy Commission. These agencies have also contributed summer grants, and the Office of Naval Research has contributed a research assistantship. This support is appreciated.

I would like to thank my wife, Jackie, for her patience and understanding.

ABSTRACT

Shock waves into argon containing a small amount of NO_2 have been used to study the kinetics of the thermal decomposition of nitrogen dioxide from 1100 to 2300°K. Mole fractions of NO_2 varied from 2.8×10^{-3} to 1.5×10^{-1}; the ratio argon/NO_2 varied from 5.6 to 360; the argon concentration varied by a factor of twenty; and the NO_2 concentration varied by a factor of ten. Under these conditions, the results indicate that two separate reaction mechanisms are operative. One path has the rate law $-d[NO_2]/dt = k_u[NO_2][A]$ with $k_u = 3 \times 10^{13} \exp[-65400/RT]$ $\underline{M}^{-1}$ sec^{-1} and is apparently the unimolecular decomposition of NO_2 at the second order limit. The other path has the rate law $-d[NO_2]/dt = k_b[NO_2]^2$ with an activation energy of 22 ± 6 kcal/mole. This path is believed to be the bimolecular decomposition of NO_2 first observed by Bodenstein. However, extrapolation of this mechanism to the shock tube temperatures gives results about eight times too low. The reason for this discrepancy is not known. One interpretation is that there is another bimolecular reaction path for the decomposition of NO_2. A good possibility for such a path is the bimolecular formation of NO_3, recently postulated by Ashmore and Levitt, and its subsequent rapid decomposition, either by reaction with NO_2 or by unimolecular dissociation into $NO_2$and O. This discrepancy has also recently been observed by Steinburg and Lyon in a con-

current investigation. However, the mechanism and conclusions of that study are not supported by the present investigation.

Part II consists of a paper that has already been published on the kinetics of the ferrous ion-oxygen reaction in sulfuric acid solution.

TABLE OF CONTENTS

I. KINETICS OF THE THERMAL DECOMPOSITION OF NITROGEN DIOXIDE BEHIND SHOCK WAVES

A. Previous Investigations

At temperatures of around 800°K and above, nitrogen dioxide is unstable thermodynamically with respect to nitric oxide and oxygen.

$$NO_2 + NO_2 = NO + O_2 + NO \qquad (1)$$

The rates of both the forward and reverse of reaction 1 have been extensively studied. Bodenstein and Ramstetter (1) used a manometric technique and observed that, between 592 and 656°K, the rate of the forward reaction was proportional to the square of the NO_2 concentration and the activation energy was 26.6 kcal/mole. Thus for this case the above stochiometric equation is, in fact, the elementary reaction. The kinetics of the reverse reaction were studied by Bodenstein and Lindner (2) from 470 to 662°K, and the reaction was found to be termolecular as written. From the known equilibrium constant, the bimolecular rate constants for the forward reaction were computed. The two sets of data form a single line on an Arrhenius plot of log rate constant versus reciprocal temperature (3). This is one of the classical demonstrations that the equilibrium constant of an elementary process is the ratio of the forward to the reverse rate constant. The combined data may be well represented by the rate expression (4):

$$k_b = 1.8 \times 10^9 \exp [-26600/RT] \ M^{-1} \ sec^{-1}$$

where k_b is the rate constant for reaction 1 in the forward direction and M signifies units of moles per liter.

The kinetics of reaction 1 have recently been studied by a spectrophotometric method by Rosser and Wise (5) between 630 and 1020°K over NO_2 concentrations of 10^{-4} to 10^{-5} M. They too report a bimolecular rate law. The combined data of all investigations fit a single straight line on an Arrhenius plot with an activation energy of 26.9 kcal/mole. Rosser and Wise found the reaction strictly homogeneous and unaffected by large pressures of the inert gases nitrogen, helium, and carbon dioxide. Their expression for the rate constant is $k_b = 4.0 \times 10^9 \exp [-26900/RT] \ M^{-1} \ sec^{-1}$.

Ashmore and Levitt (6) have reported that initial rates of nitrogen dioxide pyrolysis near 700°K are greater than the rates observed by Rosser and Wise at this temperature or the extrapolated rates of Bodenstein and Ramstetter. The reaction was followed by measuring the change in light absorption through a heated cylindrical cell with a logarithmic photometer and high speed recorder. In this way the concentration could be measured every five seconds. The initial rate was about twice as great as the rate expected from the earlier work, but the rate decreased to the expected value as the reaction proceeded. This increased initial rate was not observed when NO was present initially, so the conclusion

was drawn that the presence of NO, either added initially or due to reaction, inhibits the mechanism responsible for the increase in initial rate. Ashmore and Levitt have proposed the following mechanism involving NO_3, the nitrate free radical.

$$NO_2 + NO_2 \xrightarrow{k_2} NO_3 + NO \qquad (2)$$

$$NO_3 + NO \xrightarrow{k_3} NO_2 + NO_2 \qquad (3)$$

$$NO_3 + NO_2 \xrightarrow{k_4} NO_2 + O_2 + NO \qquad (4)$$

Reactions 3 and 4 are well known in the thermal decomposition of N_2O_5, and a recent summary of estimates of their rate constants is available (7). By combining information obtained from the shock tube investigation of the N_2O_5 decomposition by Schott and Davidson (7) and other studies, it is possible to arrive at independent values of k_2, k_3/k_4, and k_3/k_4k_2 (8) which agree fairly well with the values published by Ashmore and Levitt. These values will be considered further when attempts to extrapolate the Ashmore and Levitt mechanism to high temperatures are considered. It should be pointed out that the bimolecular path first observed by Bodenstein and Ramstetter is also occurring, and after inhibition of the Ashmore and Levitt mechanism by NO has become effective, the simple bimolecular path may be observed. Ashmore and Levitt

find the bimolecular rate constant $k_b = 19.4\ \underline{M}^{-1}\ sec^{-1}$, which agrees very well with the value 20 $\underline{M}^{-1}\ sec^{-1}$ reported by Rosser and Wise at 707°K.

The kinetics of NO_2 decomposition at the high temperatures behind shock waves was investigated briefly in this laboratory by Dr. W. R. Gilkerson in 1954. The results of this unpublished investigation were that the process had an activation energy of about 25 kcal/mole and that the reaction was proportional to the square of the total gas concentration.

As the present investigation was being conducted, a concurrent investigation of NO_2 decomposition behind shock waves was reported by Steinburg and Lyon (9). The reaction was studied in mixtures containing 1 to 3.22% NO_2 in argon over the temperature region 1400-2500°K in a three inch square shock tube. The reaction was followed by measuring the absorption of light of a small wavelength band near 436 mμ, as in the present experiments. The decomposition rate was reported to be first order in both NO_2 and argon, resulting in the rate expression $-d[NO_2]/dt = k_{SL}[NO_2][A]$. The rate constant is $k_{SL} = 3.82 \times 10^{11} \exp[-46100/RT]\ \underline{M}^{-1}\ sec^{-1}$. As will be discussed in more detail later, the two shock tube investigations give identical rates of decomposition under identical conditions. When NO_2-argon mixtures are rapidly heated and compressed by a shock wave, light emission is observed which is yellow-orange in color. Steinburg and Lyon

found the intensity of this light to follow the NO_2 concentration. This conclusion has been qualitatively verified in the present investigation.

The mechanism proposed by Steinburg and Lyon is given below.

$$NO_2 + A \xrightarrow{k_5} NO_2^* + A \qquad (5)$$

$$NO_2^* + A \xrightarrow{k_6} NO_2 + O + A \qquad (6)$$

$$NO_2^* + A \xrightarrow{k_7} NO_2 + A + h\nu \qquad (7)$$

$$NO_2 + O \xrightarrow{k_8} NO + O_2 \qquad (8)$$

From their empirical observation of a 46 kcal/mole activation energy they rule out the dissociation reaction 9 below, which has an activation energy of around 71 kcal/mole. However, the above mechanism is highly implausible, as will be discussed in detail later.

The present investigation, over wider concentration ranges, indicates that the decomposition proceeds partly via the Bodenstein mechanism and partly via the "quasiunimolecular" decomposition described by reactions 9 and 10.

$$NO_2 + A = NO + O + A \qquad (9)$$

$$NO_2 + O = NO + O_2 \qquad (10)$$

Reaction 9 is rate determining since 10 is very fast. The apparent activation energy is therefore intermediate between 26.6 and 71 kcal/mole and is dependent on the experimental conditions. Under suitable conditions in the present work, an activation energy of 57 kcal/mole was observed in experiments designed to emphasize the contribution of reaction 9. Therefore, the present investigation does not support the mechanism or the conclusions of Steinburg and Lyon.

Other investigations of nitrogen oxide reactions by the shock tube method include the study of N_2O_5 decomposition rates mentioned above (7), and the study of the room temperature decomposition of N_2O_4 to NO_2 by Carrington and Davidson (10). The fact that the latter reaction is quite rapid at room temperature means that it will have no influence upon the high temperature decomposition of NO_2.

B. The Experimental Method

1. Introduction

The thermal decomposition rate of NO_2 has been observed over the temperature range 1100 to 2300°K in a gas mixture of argon containing a small amount of NO_2. The high temperatures result from passage of a plane shock wave through the gas mixture contained in a shock tube. The NO_2 mole fractions ranged from 2.8×10^{-3} to 1.5×10^{-1}, and initial pressures of NO_2-argon mixture ranged from .01 to .1 atm. The pressure and density ratios across the shock depend on the shock speed and composition of gas. The NO_2 concentration behind the shock wave varied from about 7.8×10^{-5} to about 8.0×10^{-4} M or a factor of ten. The argon concentration varied from 1.5×10^{-3} to 3.0×10^{-2} M or a factor of twenty. The ratio argon/NO_2 varied from 5.6 to 360 or a factor of sixty-five. Final pressures behind the shock wave varied from .23 to 4.4 atm.

The general technique of studying fast reactions behind shock waves, as previously developed in this laboratory, has been used (11). The shock wave is generated in a shock tube--a long, cylindrical tube separated into two sections by a diaphragm of easily ruptured material. Gases such as helium and hydrogen are placed in one section at high pressure, and the gas under investigation is placed in the other section at a lower pressure. When the diaphragm is ruptured,

a shock wave is propagated into the gas under study, which imparts a large amount of enthalpy to an element of the gas in the time of a few collisions. If observations are made at a place sufficiently far removed from the diaphragm so that the wave has become stable, all the gas parameters immediately behind the wave are constant and may be calculated from the initial conditions and one property of the shock wave. The property is usually the incident shock wave speed. The calculation assumes that equilibrium is established in the time of a few collisions, and for many gases this assumption is found to be true over a wide temperature range. However, processes such as chemical reaction, ionization, or vibrational relaxation may require a certain observable time to reach equilibrium, so it is in principle possible to study these events. Also, the temperature and density behind the shock wave change as these processes occur, since a change in enthalpy is involved. In the present case, the reaction is endothermic, and the temperature and density would change greatly behind the shock front if pure NO_2 were placed in the tube. This would greatly complicate determination of the rate constant at a certain temperature, so a small amount of NO_2 and a large amount of argon is used instead. The shock wave properties are largely determined by the argon, and this "heat buffer" greatly decreases the temperature and density changes behind the shock wave. In the current experiments, the change in light absorption by NO_2 due to chemical

reaction was observed with a photomultiplier-oscilloscope combination.

The reflected shock wave region has also been used in the present investigation in addition to the incident shock wave region discussed in the last paragraph. The reflected shock wave processes the hot compressed gas behind the incident shock wave, and therefore temperatures and pressures in this region are much larger than behind the incident shock wave. It is possible to adjust conditions so that no reaction occurs behind the incident shock but only behind the reflected shock. Therefore, much larger argon/NO_2 ratios and temperatures are possible with the same equipment. The calculation of gas parameters behind incident and reflected waves will be discussed in detail in a later section.

2. Wave Motion in a Shock Tube

Shock wave methods offer a way of studying the rates of rapid gas phase reactions. The waves may be easily generated in a shock tube by allowing a high pressure gas originally in the driver section to push on the gas under investigation at a lower pressure in the shock wave section. Rupture of the diaphragm between these two sections causes a flow pattern which may be shown ideally on an x,t diagram (figure 1) of distance along the tube, x, plotted against t, the time after rupture of the diaphragm. The dimensions are those of the shock tube used in the present study, and the waves shown result from hydrogen at .57 atm in the driving section and argon at .04 atm in the shock wave section. This results in temperatures of 1341°K behind the incident shock and 2745°K behind the reflected shock if room temperature is 300°. The diagonal lines represent various disturbances moving through the gas; the reciprocal of the slope of the line gives its speed. Pressure profiles at various times are also shown.

When the diaphragm is removed, the high pressure gas pushes on the low pressure gas like a piston, causing a shock wave to move out into the gas. The shock wave compresses and imparts a large amount of enthalpy to an element of the gas. It moves into the gas under investigation with a speed, S, intermediate between the speed of sound in the cool, unshocked gas and the hot, shocked gas. Any compres-

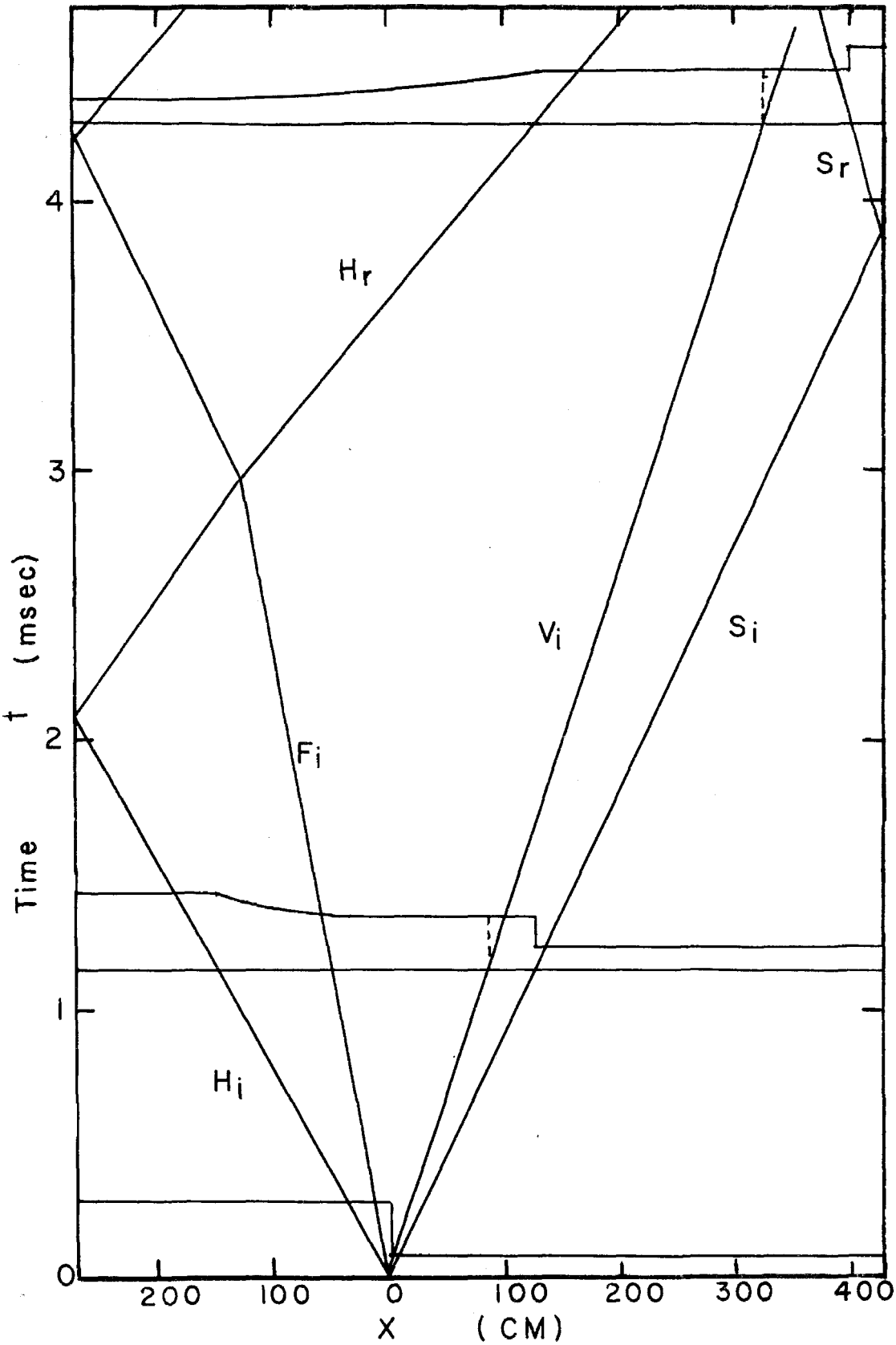

Figure 1. Shock Tube Flow Pattern

sion wave generated behind the shock wave will travel with the faster sonic speed in the hot gas and will overtake the shock front. Therefore, the shock front is self-sharpening, and even though the diaphragm does not shatter uniformly, a steady shock wave will result--empirically in a distance of ten or fifteen tube diameters. The temperature, density and pressure change as step functions across the shock front in a manner which may be calculated.

The gas behind the incident shock wave is set in motion with the speed v. Also, the original interface between the two gases moves into the shock wave section with the speed v of the gas flow behind the incident shock wave. In front of this interface is the hot, compressed gas under investigation; behind is the cool, expanded driving gas. The interface is not self-sharpening and spreads out by turbulent mixing of the two gases. Arrival of this "cold front" at an observation port therefore concludes an experiment; however, reflected shock waves may arrive first depending upon the geometry of the experiment.

The incident shock wave is reflected from the closed end of the tube as a second shock wave which travels through the once shocked gas, again sharply raising the temperature, density, and pressure. The gas behind the reflected shock, however, is at rest with respect to the shock tube. The gas parameters may be known in this region, and in this investigation both incident and reflected waves were used with the

same results under identical conditions.

An expansion wave travels into the high pressure gas in the driver section with the local sonic speed. This wave broadens with time, as the foot of the wave must travel with the lower sonic speed of the expanded, cool gas which is flowing toward the shock wave section. The head of the expansion fan is reflected from the end of the driver section as an expansion wave whose head moves into the shock wave section with a speed equal to the gas flow speed plus the local sound speed. This expansion wave could therefore overtake and dissipate the shock wave, so the driver section is made long enough to prevent interference from this wave. The relationships between these disturbances may be seen on the x, t diagram (figure 1). Methods of calculating the wave speeds and parameters of gases behind incident and reflected shock waves are described below.

The motion shown in the x, t diagram is for an ideal case in which the shock wave is set up instantly, and no energy is required to remove the diaphragm. In practice, the wave is usually somewhat weaker than predicted from the initial pressure ratio. The usual procedure is to work many tube diameters below the diaphragm and to base calculations on the measured speed of the shock front near the observation port. Experimental study of other dissipative effects in real gases has established that the simple equations neglecting

heat flow and viscosity are satisfactory. Many investigations have considered these problems; references 12, 13, and 14 are a few selected examples.

3. Observations of Rapid Events behind Shock Waves

The thermal decomposition rate of NO_2 was measured by observing the change in light absorption through the NO_2-argon mixture in the shock tube with time. The sources of radiation were lines isolated from mercury arcs with interference filters. Nitrogen dioxide absorbs strongly from around 300 to 550 mμ (15), and mercury lines near 405, 436, and 546 mμ are satisfactory. A one mm wide sheet of this light passes through the shock tube and falls on the cathode of a photomultiplier.

The photocurrent is displayed as the vertical deflection of an oscilloscope trace. Photographs of a single oscilloscope sweep beginning just before the shock wave passes a given station therefore give a record of light intensity as a function of time.

Typical oscilloscope traces are shown in figure 2 for incident and reflected shock waves. As the shock wave passes before the observing station, the gas is compressed, and the signal is deflected upward, corresponding to smaller light transmission. As NO_2 disappears by reaction and forms the transparent products NO and O_2, the light transmission increases, and the trace moves lower. At sufficiently low temperatures, no reaction is observed (figure 2 (a) and (d)). The fact that this signal is constant proves that the conditions behind the shock wave are somewhat uniform. A slow and fast reaction behind incident shock waves (figure 2 (b) and (c)) illustrates typical experimental observations. The

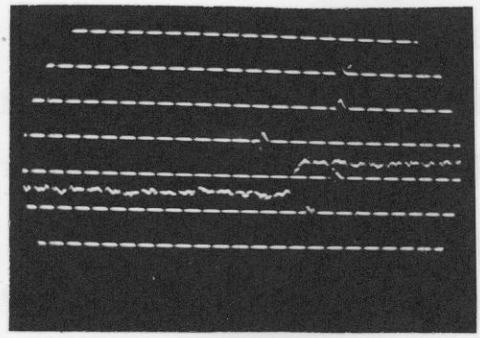

a

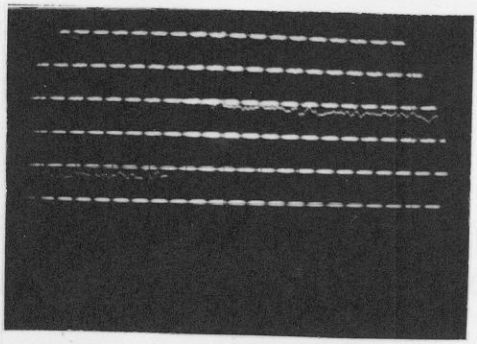

b

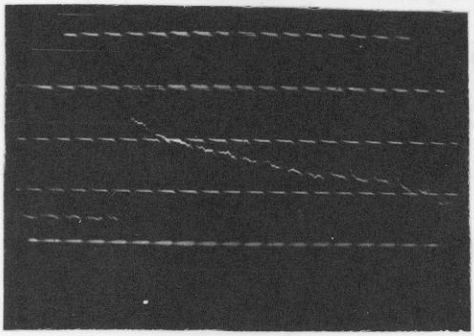

c

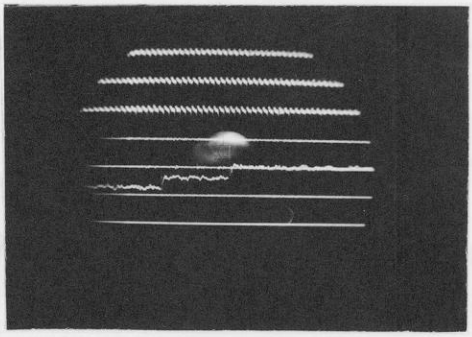

d

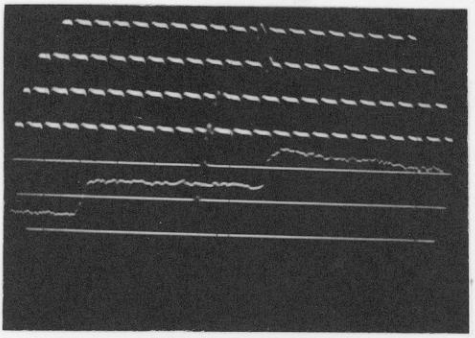

e

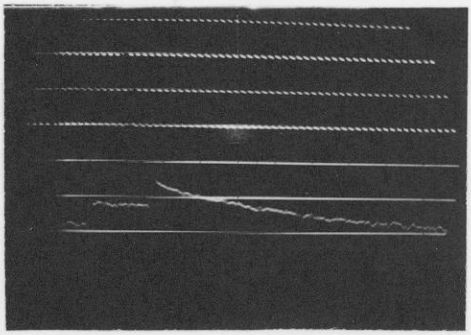

f

Figure 2. Typical Oscilloscope Records

Figure 2. (continued). Typical Oscilloscope Records Timing marks every 10 μsec.

(a) Constant absorption before and after passage of the shock wave; T_i = 844°K; initial pressure = .04 atm; mole fraction NO_2 = .023; λ = 436 mμ.

(b) Slow reaction; T_i = 1431°K; initial pressure = .02 atm; mole fraction NO_2 = .0500; mole fraction NO = .0430; λ = 436 mμ.

(c) Fast reaction; T_i = 1695°K; initial pressure = .02 atm; mole fraction NO_2 = .0504; λ = 405 mμ.

(d) Constant absorption behind incident and reflected shock waves; T_r = 932°K; T_i = 583°; initial pressure = .04 atm; mole fraction NO_2 = 7 x 10^{-3}; λ = 436 mμ.

(e) Slow reaction behind reflected shock; T_r = 1716°K; T_i = 952°; initial pressure = .019 atm; mole fraction NO_2 = .0234; λ = 436 mμ.

(f) Fast reaction, no reaction occurs behind incident shock; T_r = 1682°K; T_i = 899°; initial pressure = 0.1 atm; mole fraction NO_2 = 2.8 x 10^{-3}; λ = 436 mμ.

remaining two photographs (figure 2 (e) and (f)) illustrate reactions behind reflected shock wave, and it may be seen that no reaction takes place behind the incident wave. Other sweeps are for calibration of the photocurrent, and the timing marks are ten μsec apart in all cases.

4. Instruments and Procedures

The experiments reported here were done in a 15 cm diameter shock tube of aluminum and pyrex glass pipe. The lengths of the driving section and the shock wave section were increased about 50 percent over the tube previously described (11). The driving section was a 270 cm aluminum pipe, while the shock wave section consisted of a 140 cm aluminum pipe and two 150 cm pyrex glass pipes. Optical measurements were made directly through the pyrex glass pipe. The sections were sealed with "O" rings lubricated with silicone stopcock grease (Dow Corning Company) and held together with standard glass pipe flanges. For experiments behind incident shock waves, the ends of the driver and shock wave sections were closed with flat plates. For experiments with reflected shock waves, a special end plate was used which placed the reflecting surface about 12 centimeters in front of the end of the glass pipe. The clearance between the circumference of this plate and the inside glass wall was about one mm. A plunger arrangement allowed the portion of the shock tube behind the reflecting surface to be evacuated through a hole in the reflecting plate. This opening could then be closed immediately before the diaphragm was burst. The reflecting surface was about 3 cm from the station at which observations of the reflected shock were made.

The shock wave section of the tube could be pumped to below 0.1 μ mercury pressure, but usual practice was to

evacuate to 1μ pressure before placing the NO_2-argon mixture in the tube. The pumping time in this case was around eight hours, and this long time was the limiting factor in collecting data. A mercury diffusion pump, protected with liquid nitrogen at all times, was used to evacuate the shock wave section. A mechanical oil pump evacuated the driving section. The leak rate was measured at various times, and a value of 0.05μ/min was typical. Apiezon N grease was used on the stopcocks. Cellulose acetate sheets were used for diaphragm material and were usually burst by touching with a needle. The pressure of NO_2-argon mixture in the shock tube was measured with a butyl phthalate manometer, while the high pressures of the driving section were measured approximately with spring type dial gauges.

Two types of mercury arc lamps were used as sources for the photoelectric observation of NO_2 concentration. In practically every experiment, a Hanovia Type SH quartz lamp (No. 5352) was operated from a 120 volt battery bank at 150 watts. The 436 mμ line was isolated, and the light intensity was measured with an RCA 931-A photomultiplier. In several early experiments, an Osram HBO 200 high pressure d.c. mercury arc operated as described previously was used (16). The 405 mμ line was isolated, and an RCA 1P28 photomultiplier was used. The 1P28 tube is the 931-A with a quartz jacket to improve the ultraviolet sensitivity. This arc became unstable in operation, and the Hanovia arc was then used

exclusively. Experiments with higher concentrations of NO_2 used the 546 mμ line isolated from the Hanovia lamp and collected on a 931-A photomultiplier.

Filter combinations found useful in this work are presented below.

Wave length (mμ)	Interference filter	Corning cutoff filter	Half maximum width (mμ)
405	405 (B & L)	3060	11
436	436 (B & L)	3060	10
546	546 (Baird) (monolayer)	3486	15

The various light beams through the Pyrex shock tube passed three one mm slits before falling on the photomultiplier. The optical instrumentation has been previously described and was used unchanged in the present experiments (17).

In experiments behind both incident and reflected shock waves, the speed of the incident shock wave front was measured to provide the extra condition needed to solve the shock wave equations. This speed was measured by an optical method--based on the schlieren effect--between two stations on the optical bench 30.00 cm apart. The rapid change in density as the shock wave passes an observation station will deflect a light ray several degrees toward the upstream side. Light beams are positioned on the three slit optical path so that they partly go through the last slit and partly fall on the upstream side of the slit. As the shock wave passes

before a timing station, the amount of light passing through the last slit and falling on the photomultiplier changes rapidly. This give a sharply rising signal which may be amplified and used to switch a timing circuit. The light sources are 500 watt tungsten filament projection lamps operated at 120 volts d.c.; the photomultipliers are 931-A tubes. The sharply rising signal from the photomultiplier triggers a pulse from a monostable multivibrator (univibrator) circuit. This "flip-flop" circuit effectively amplifies the pulse so that it may be used to switch a crystal controlled timing circuit (Potter Model 456 1.6 megacycle counter chronograph). Blue cobalt glass filters were used to make the intensity of the tungsten lamps comparable with the mercury arcs. The total change in intensity of the triggering light beam is enhanced by the light absorption of NO_2 behind the shock wave.

In addition to switching the timer, the pulse from one timing station was used to trigger a single sweep on either one or both of two oscilloscopes available (Tektronix, model 512). This negative pulse is taken from the circuit at the plate of a thyratron (6D4) inserted after the stage from which the timer pulse is taken. The relatively slow recovery time of the thyratron insures that extraneous sweeps will not be triggered after the passage of the shock. Such triggering might occur from passage of reflected shock waves, various expansion waves, or bits of membranes in front

of the light beam. The oscilloscope sweep was triggered by the first timing station when the reaction was observed behind incident shock waves. The reaction was followed at one of the two stations between the timing stations. When the reaction was followed behind reflected shocks, the timing station which cut off the timer started the sweep. The reaction was followed at a station between the last timing station and the reflected shock end plate. This enables the reaction to be followed before boundary layers grow too large.

The photomultipliers were operated so that 100 microamperes of plate current were drawn through a plate resistor of 10^4 ohm, and therefore the deflection on the scope was about one volt. The plate of the photomultiplier was connected to the vertical amplifier input of the scope with about three feet of low capacitance coaxial cable (13 $\mu\mu$f/ft). The scope presents a capacitance of 45 $\mu\mu$f in the vertical amplifier circuit. Therefore, the rise time of the photomultiplier-scope combination should be about one microsecond. All electronic equipment was given time to become thoroughly stable in operation before an experiment was performed. The change in current through the photomultiplier as the shock passes would tend to change the voltage across each dynode stage. This voltage controls the total amplification of the signal and is typically 60 volts per stage in these experiments. The effect is most serious in the last few

dynode stages, where the space current is an appreciable fraction of the total current through the tube. Therefore, the voltage is held fixed across the last three dynodes for a few milliseconds by suitable capacitors.

Photographs of the sweeps and calibration marks were made on the very fast Kodax Linagraph Pan 35 mm film. These photographs were accurately traced from enlarger projections. Light intensity values at various times were measured from the tracings.

The calibration procedure for interpreting vertical deflection measurements is described by G. Schott (16). The photomultiplier output enters the scope vertical amplifier circuit at one terminal of the difference amplifier, and a dry cell is connected to the other terminal. Immediately after completion of the experiment, the photomultiplier cable is replaced by a connection to ground, and sweeps at various accurately known fractions of the dry cell voltage are photographed. The voltage is measured with a Helipot precision potentiometer. The photocurrent values as a function of time can then be obtained. It is necessary that the scope does not change in sensitivity between the photomultiplier record and the calibration records. It will be noticed that no scope control must be used to carry out this procedure. An important precaution is that the grid of the side of the difference amplifier that is not used during the calibration must not be allowed to float, but must be

connected to ground. The scopes used in this investigation--when operated so that the input signal was d.c. coupled to the vertical amplifier--have the annoying feature that rapid changes in d.c. level are not measured accurately. The correct d.c. value is not reached for several seconds. The discrepancy was found to be typically 3%, and corrections for this "d.c. shift" were applied to all photomultiplier records. Timing marks were placed on the photomultiplier and calibration sweeps by applying pulses to the cathode of the cathode ray tube every ten microseconds from a crystal controlled 100 kilocycle circuit.

5. Reagents

Nitrogen dioxide (The Matheson Company) was purified using the method of reference (16). Oxygen (Linde) was passed through a dry ice trap filled with glass wool and then was bubbled through liquid NO_2 in an ice-salt bath. The liquid was initially dark blue-black due to the presence of N_2O_3, but became light yellow in color, since the NO present had either been swept out or oxidized. At this stage, the oxygen stream saturated with NO_2 vapor was diverted to a train consisting of P_2O_5 coated glass beads and a storage trap on the vacuum line. After the NO_2-O_2 stream had swept through the trap about five minutes, collection of the NO_2 was begun. It was frozen out as a very pale yellow solid in the storage trap by a dry ice-trichloroethylene bath. About two-thirds of the liquid NO_2 remaining in the ice-salt bath was distilled in the stream of O_2 into the storage trap. The oxygen was then pumped off, and the NO_2 was stored as a solid under dry ice.

Nitric oxide (The Matheson Company) was purified by distillation, and the main impurity was NO_2. Nitric oxide was condensed under liquid N_2 in a trap on the vacuum line as a green, brown, blue, and white solid. The material was then distilled twice from the liquid at about -150°C to a trap cooled with liquid N_2 at -196°C. The temperature of the NO-N_2O_3 solution was not easy to control by lowering the liquid N_2 level in a dewar flask. The resulting dangerously

large vapor pressure could blow out stopcocks. A methylpentane bath (Phillips Petroleum Company, Methylpentanes, commercial grade) which had been cooled with a liquid N_2 cold finger is usable to around -160°C and is very satisfactory for holding the liquid NO-N_2O_3 at -160 to -150°C, where the vapor pressure of NO above the solution is in the one atmosphere range. After the second distillation the solid was a uniform very light gray which melted to give a light greenish-blue liquid.

Mixtures of NO_2 and argon were prepared as needed and stored in a 22 liter bulb covered with black cloth to prevent photodecomposition from the room fluorescent lamps. As many as twenty and as few as two shock tube fillings could be stored. The NO_2 under dry ice in the storage trap was pumped on briefly with the mercury diffusion pump and then was allowed to melt. The manifold and storage bulb were conditioned by allowing about 30% of the final NO_2 pressure to stand in the system for about ten minutes and then pumping this gas out. Next, NO_2 was allowed to flow into the bulb to the desired pressure, as determined by a butyl phthalate manometer. The storage bulb stopcock was closed, and the NO_2 in the vacuum manifold was pumped out. Argon (Linde, 99.92% pure, principal impurity N_2) was used without further purification and was added to the manifold in such a way that a small positive pressure was always maintained in the argon line. About .8 atm argon, as measured with a

mercury manometer, was placed in the manifold, and then the storage bulb stopcock was opened slightly. Argon at the much higher pressure filled the bulb, and no NO_2 escaped. When the pressure reached one atm, the manifold was isolated from the argon supply. About 15 seconds were allowed for the NO_2 and argon pressure inside the bulb to slightly adjust to the argon pressure in the manifold, and then the storage bulb stopcock was closed. The manifold pressure was then the total pressure in the storage bulb.

It was necessary to correct for the N_2O_4 present to determine the formal mole fraction of NO_2. Values of the equilibrium constant for the reaction

$$2NO_2 = N_2O_4$$

were taken from Yost and Russell (18). By combining the results of several investigations, they recommend ΔF°_{298} = -1110 cal, ΔH°_{298} = -13693 cal, for the reaction as written above. The equilibrium constant is therefore $K_{298} = P_{N_2O_4}/P_{NO_2}^2 = 6.51\ atm^{-1}$. This constant was corrected to the measured room temperature. The formal NO_2 mole fraction is then the NO_2 mole fraction plus twice the N_2O_4 mole fraction.

The NO-NO_2-argon mixture was prepared by flowing NO to the desired pressure into the storage bulb using the butyl phthalate manometer. Then an NO_2 pressure over twice as great was placed in the manifold, and the storage bulb

stopcock was slightly opened, allowing the NO_2 to flow into the storage bulb with a higher pressure in the manifold. The total pressure of NO_2 and NO was then measured by allowing the manifold and bulb pressures to equalize as explained above. Then argon was placed in the bulb as before. In all cases, the contents of the bulb were allowed over eighteen hours to mix before being used for an experiment.

6. Calculation of Gas Parameters behind Incident and Reflected Shock Waves

The gas parameters behind plane incident and reflected shock waves may be calculated from a knowledge of the initial temperature, initial pressure, initial composition and one property of the shock wave--almost invariably the incident shock speed. The equations of flow through a shock front--the Rankine-Hugoniot conditions--state that mass, momentum and energy are conserved in the process. The equation of state of the material must also be known. Since one is mainly concerned with the properties of an inert gas at high temperatures and low pressures, the perfect gas law is used. The reflected shock parameters may be obtained from the additional condition that the gas behind the reflected shock front has no material velocity. Discussions of solution of the shock wave equations for the case of a reacting gas have been given previously (17), so the present discussion will refer almost exclusively to the system of this investigation.

The Rankine-Hugoniot conditions will be set up initially with respect to a stationary shock front--either incident or reflected. The velocities concerned are shown below both for shock stationary coordinates and for laboratory coordinates; the vertical lines denote the shock front.

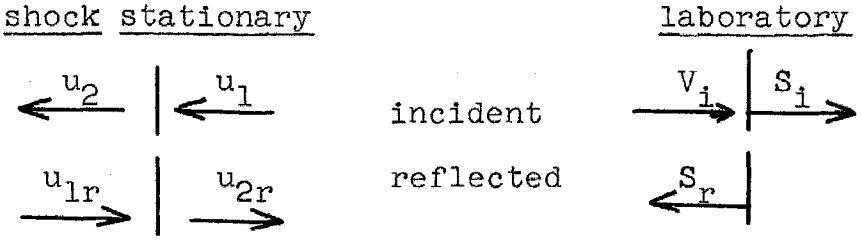

The subscript 1 refers to gas through which the wave has not passed; subscript 2 refers to shocked gas. Subscript i refers to incident shocks, and subscript r refers to reflected shocks. The speeds u refer to material or gas flow speeds relative to the shock front. The speeds of the shock fronts are denoted by S, and v_i refers to the material speed, all in the laboratory system. The gas is not flowing in the laboratory coordinates before the passage of the incident shock and behind the reflected shock. Therefore, the two sets of speeds are related by the expressions below.

$$S_i = u_1 \qquad\qquad S_r = u_{2r}$$

$$v_i = u_1 - u_2 \qquad\qquad S_r + v_i = u_{1r}$$

The magnitudes are correctly given by the equations presented; the directions of the motions are shown in the diagram above.

The Rankine-Hugonoit conditions in the shock stationary coordinates are:

$$\rho_1 u_1 = \rho_2 u_2 \qquad \text{mass} \qquad (11)$$

$$\rho_1 u_1^2 + P_1 = \rho_2 u_2^2 + P_2 \qquad \text{momentum} \qquad (12)$$

$$h_1 + \tfrac{1}{2}u_1^2 = h_2 + \tfrac{1}{2}u_2^2 \qquad \text{energy} \qquad (13)$$

In these expressions, ρ is the gas density, P is the pressure, and h is the enthalpy per gram. The ideal gas equation

for one mole of gas of molecular weight W is:

$$\frac{P}{\rho} = \frac{RT}{W} \tag{14}$$

It is convenient to use the ratios given below.

$$\pi_i = \frac{P_2}{P_1} \qquad \pi_r = \frac{P_r}{P_2} \qquad \pi_T = \frac{P_r}{P_1}$$

$$\Delta_i = \frac{\rho_2}{\rho_1} \qquad \Delta_r = \frac{\rho_r}{\rho_2} \qquad \Delta_T = \frac{\rho_r}{\rho_1}$$

$$\Theta_i = \frac{T_2}{T_1} \qquad \Theta_r = \frac{T_r}{T_2} \qquad \Theta_T = \frac{T_r}{T_1}$$

The perfect gas equation for one mole then simplifies to:

$$\pi = \Delta \Theta \tag{15}$$

From the Rankine-Hugoniot relations and the ideal gas expression, the incident shock speed, S_i, is found to be given by:

$$S_i^2 = \frac{RT_1}{W} \quad \frac{(\pi_i - 1)\,\Delta_i}{(\Delta_i - 1)} \tag{16}$$

The material speed behind the incident shock wave is:

$$v_i = S_i \left(1 - \frac{1}{\Delta_i}\right) \tag{17}$$

The enthalpy change per gram across the shock front is:

$$h_2 - h_1 = \frac{1}{2}\frac{RT_1}{W}\ (\Pi_i - 1)\left(1 + \frac{1}{\Delta_i}\right) \qquad (18)$$

which may be rearranged with the aid of the perfect gas law to give:

$$\Pi_i = \frac{2W}{RT_1}\ (h_2 - h_1) + 1 - \theta_i + \frac{1}{\Delta_i} \qquad (19)$$

If the necessary enthalpies are known, 18 can be applied to shock waves in any gas. The reciprocal density ratio $1/\Delta_i$ is very insensitive to changes in the temperature and is small, so 18 or 19 is usually solved for a given enthalpy and temperature ratio at an approximate $1/\Delta_i$. The correct $1/\Delta_i$ is then found readily by iteration. One then has values of Π_i, Δ_i, and θ_i from which S_i and v_i may be calculated. For the inert gases, $h = (5/2)\ (RT/W)$, and 19 becomes with this substitution:

$$\Pi_i = 4\ (\theta_i - 1) + 1/\Delta_i \qquad (20)$$

Extensive tables of incident shock wave parameters in dimensionless form for perfect monoatomic and diatomic gases exist (19).

The gas parameters behind reflected shocks may be obtained in simple closed form for the case in which the heat

capacity does not change with the temperature (13). In this case, the enthalpy is given by:

$$h = c\,\frac{P}{\rho} = \frac{\gamma}{\gamma-1}\,\frac{P}{\rho} = \frac{\mu+1}{2}\,\frac{P}{\rho} \qquad (21)$$

The various heat capacity expressions are:

$$c = \frac{C_P}{R} \qquad \gamma = \frac{C_P}{C_V} \qquad \mu = \frac{\gamma+1}{\gamma-1}$$

The Rankine-Hugoniot relations then give the following expressions for any shock wave.

$$\Delta = \frac{\Pi\mu + 1}{\Pi + \mu} \qquad (22)$$

$$\Theta = \frac{\Pi(\Pi+\mu)}{\Pi\mu + 1} \qquad (23)$$

The incident shock imparts the material speed v_i to the still gas, and the reflected shock reduces this speed back to zero again. The following expression is defined.

$$\Phi = \left[\frac{\text{change in flow speed across shock front}}{\text{sound speed ahead of shock front}}\right]^2$$

For incident and reflected shock waves, respectively:

$$\Phi_i = \frac{v_i^2}{a_1^2} = \frac{(\Pi_i - 1)^2(\mu-1)^2}{(\Pi_i\mu+1)\,(\mu+1)} \qquad (24)$$

$$\Phi_r = \frac{v_i^2}{a_2^2} = \frac{(\pi_r - 1)^2(\mu - 1)^2}{(\pi_r \mu + 1)(\mu + 1)} \tag{25}$$

The speed of sound, a, is $(\gamma P/\rho)^{\frac{1}{2}}$, and a_2^2/a_1^2 is θ_i. Combining 24 and 25 and substituting 23 gives a quadratic equation in π_r.

$$\frac{(\pi_i - 1)^2}{\pi_i(\pi_i + \mu)} = \frac{(\pi_r - 1)^2}{(\pi_r \mu + 1)} \tag{26}$$

The roots of this equation are:

$$\pi_r = \frac{\pi_i(\mu + 2) - 1}{\pi_i + \mu} \tag{27}$$

$$\pi_r = \frac{1}{\pi_i}$$

The second solution is unacceptable physically.

From the first Rankine-Hugoniot condition applied to the reflected shock:

$$\Delta_r = \frac{u_{1r}}{u_{2r}} = \frac{S_r + v_i}{S_r} = \frac{\pi_r \mu + 1}{\pi_r + \mu} \tag{28}$$

Substitution of v_i from 17 and π_r from 27 gives the reflected shock speed as a function of S_i, π_i and μ.

$$S_r = \frac{S_i\ (2\pi_i + \mu - 1)}{(\mu\pi_i + 1)} \tag{29}$$

Substituting 27 in 22 gives:

$$\Delta_r = \frac{\pi_i(\mu + 1)}{2\pi_i + \mu - 1} \tag{30}$$

The perfect gas equation gives the final expression:

$$\Theta_r = \frac{\pi_r}{\Delta_r} \tag{31}$$

Therefore, if the parameters of the initial shock wave into the gas are known, the reflected parameters may be obtained. Values of the reflected shock wave parameters in argon over a reflected temperature range of 850-2750°K are given in Table 1. Since only small NO_2 concentrations were used in the reflected shocks, no calculation of reflected parameters with added NO_2 was made.

Solution of the shock wave equations for a reacting gas is more involved than the cases so far discussed where the enthalpy is directly proportional to the temperature. It is desired to find π_i, Δ_i and S_i for chosen θ_i for various initial compositions and amounts of reaction. The change in enthalpy across the shock front is a function of these variables. The initial temperature in all shock calculations was assumed to be 300°K, and the measured room temperature was

never far from this value. The derivation below refers to incident shocks only, and the subscripts i have been eliminated.

The molar enthalpy of mixtures of NO_2 in argon at 300°K is:

$$H_{T_1} = \frac{(1-\phi)\mathcal{H}_A RT_1 + \phi\left[(1-\alpha_1)\mathcal{H}_{NO_2} RT_1 + (\alpha_1/2)\mathcal{H}_{N_2O_4} RT_1 + \alpha U_a\right]}{1 - (\alpha_1/2)\phi} \quad (32)$$

The symbols are defined as follows:

H_{T_1} = molar enthalpy at temperature T_1

ϕ = formal mole fraction NO_2

α_1 = degree of association of NO_2 to N_2O_4 in the reaction $NO_2 = 1/2\ N_2O_4$

U_a = ΔH_o° of above reaction = -7300 calories

$\mathcal{H}$ = $(H_T - H_o^\circ)/RT$

The denominator gives the number of moles present as a function of α_1 and ϕ for an initial amount of one mole of NO_2. The molecular weight of the gas mixture--the weight which contains Avagadro's number of molecules--is given by:

$$\overline{W}_{\alpha_1} = \frac{(1-\phi)W_A + \phi(1-\alpha_1)W_{NO_2} + (\phi/2)\alpha_1 W_{N_2O_4}}{1-(\alpha_1/2)\phi} \tag{33}$$

$$= \frac{W_A + \phi(W_{NO_2} - W_A)}{1-(\alpha_1/2)\phi} = \frac{\overline{W}_1}{1-(\alpha_1/2)\phi}$$

Therefore, $\overline{W}_1$ is the molecular weight for the case of no association to N_2O_4. The enthalpy per gram at 300°K is accordingly:

$$h_{T_1} = \frac{1}{\overline{W}_1}\left\{(1-\phi)\mathcal{H}_A RT_1 + \phi\left[\mathcal{H}_{NO_2,T_1}RT_1 + \alpha_1 U_a\right]\right\} \tag{34}$$

The enthalpy $\mathcal{H}_{N_2O_4}$ has been set equal to $2\mathcal{H}_{NO_2}$.

At the high temperatures of the gas behind the shock front, NO_2 is reacting to give NO and O_2--the thermodynamically stable products. The small fraction of N_2O_4 reacts very rapidly to give NO_2 and need not be considered. The process is represented stoichiometrically by:

$$NO_2 = NO + \frac{1}{2}O_2 \tag{35}$$

The standard enthalpy of this process at zero degrees is $\Delta H_o^\circ = U_d = 12{,}795$ cal/mole. If the degree of reaction

in 35 is α_2, the expressions analogous to 33 and 34 are:

$$h_{T_2} = \frac{1}{\bar{W}_2}\left\{(1-\Phi)\mathcal{H}_A RT_2 + \Phi\left[(1-\alpha_2)\mathcal{H}_{NO_2 T_2} RT_2 + \alpha_2 \mathcal{H}_{NO\,T_2} RT_2 + (\alpha_2/2)\mathcal{H}_{O_2 T_2} RT_2 + \alpha_2 U_d\right]\right\} \tag{36}$$

$$\bar{W}_2 = (1-\Phi) W_A + \Phi\left[(1-\alpha_2) W_{NO_2} + \alpha_2 W_{NO} + (\alpha_2/2) W_{O_2}\right] \tag{37}$$

The perfect gas law for this situation is:

$$\Pi = \left(1 + \frac{\alpha_2 \Phi}{2}\right)\Delta\Theta \tag{38}$$

The enthalpy per gram at the two temperatures, 34 and 36, and the ideal gas law, 38, may be substituted into 18 and rearranged to give the final expression.

$$\Pi = -\left[1 + (\alpha_2/2)\Phi\right]\Theta + 1 + 1/\Delta + 5(1-\Phi)\left[(\bar{w}_1/\bar{w}_2)\Theta - 1\right] + 2\Phi(\bar{w}_1/\bar{w}_2)\left\{(1-\alpha_2)\mathcal{H}_{NO_2 T_2}\Theta + \alpha_2 \mathcal{H}_{NO\,T_2}\Theta + (\alpha_2/2)\mathcal{H}_{O_2 T_2}\Theta + (\alpha_2 U_d / RT_1)\right\} - 2\Phi\left\{\mathcal{H}_{NO_2 T_1} + (\alpha_1 U_a / RT_1)\right\} \tag{39}$$

When the degree of reaction α_2 is zero--immediately after passage of the shock front--the final expression is:

$$\pi = 1 - \theta + 1/\Delta + 5(1-\phi)(\theta-1) + 2\phi\left\{\gamma_{NO_2 T_2}\theta - \gamma_{NO_2 T_1} - (\alpha_1 U_a / R T_1)\right\} \quad (40)$$

The expressions 39 and 40 were solved for π and Δ, by the iterative process previously described, for each mixture composition and initial pressure at zero and fifty percent reaction. This calculation was generally done at the four temperatures 1000, 1500, 2000, and 2500°K. Values of S_i could be calculated at these temperatures, and values of S_i at intermediate temperatures could be found on plots of T_2 against S_i^2, which are linear over this range. The values of T_2 for each experiment were found from large graphs of T_2 against S_i. The value of Δ_i for α_2 equal zero at various values of T_2 was found to the accuracy required from smooth curves of Δ_i for the NO_2-argon mixtures minus Δ_i for pure argon plotted against T_2. When NO is also present initially, its contribution to the enthalpy must be considered in a way which is analogous to the case with added NO_2 presented above. Values of gas parameters behind incident shock waves calculated for compositions used in this investigation are presented in Table 2.

Thermodynamic properties of NO and O_2 over a wide

temperature range have been obtained from NBS tables, Series III (20). The corresponding properties of NO_2 were taken from NBS-NACA tables (21). Values of $\Delta H_o^\bullet$ were taken from Series I of the NBS tables (22).

The gas parameters behind the reflected shock wave are calculated from the measured incident shock wave speed. The photoelectric records of intensity versus time for reflected shock wave experiments may be used to obtain an observed reflected shock speed. This speed may be compared with the reflected shock speed calculated from the observed incident shock speed. As shown in figure 2, the time between passage of the incident and reflected shock waves is the length of the "plateau" between the two upward deflections. With the distance between the observation slit and the reflecting surface and the observed incident shock speed known, the reflected shock speed may be easily calculated. Figure 3 represents S_r, the reflected shock speed, versus $T_r/T_2 = \theta_r$, the temperature ratio between once and twice shocked gas. The curve refers to speeds calculated from the measured incident shock speed; the points refer to speeds measured from the photoelectric records. The approximate agreement between these quantities is comforting. The values shown in figure 3 are tabulated as table 3.

A further indication that viscosity and heat conduction effects do not invalidate experiments behind reflected shock waves is the observation that rate constants are the same to

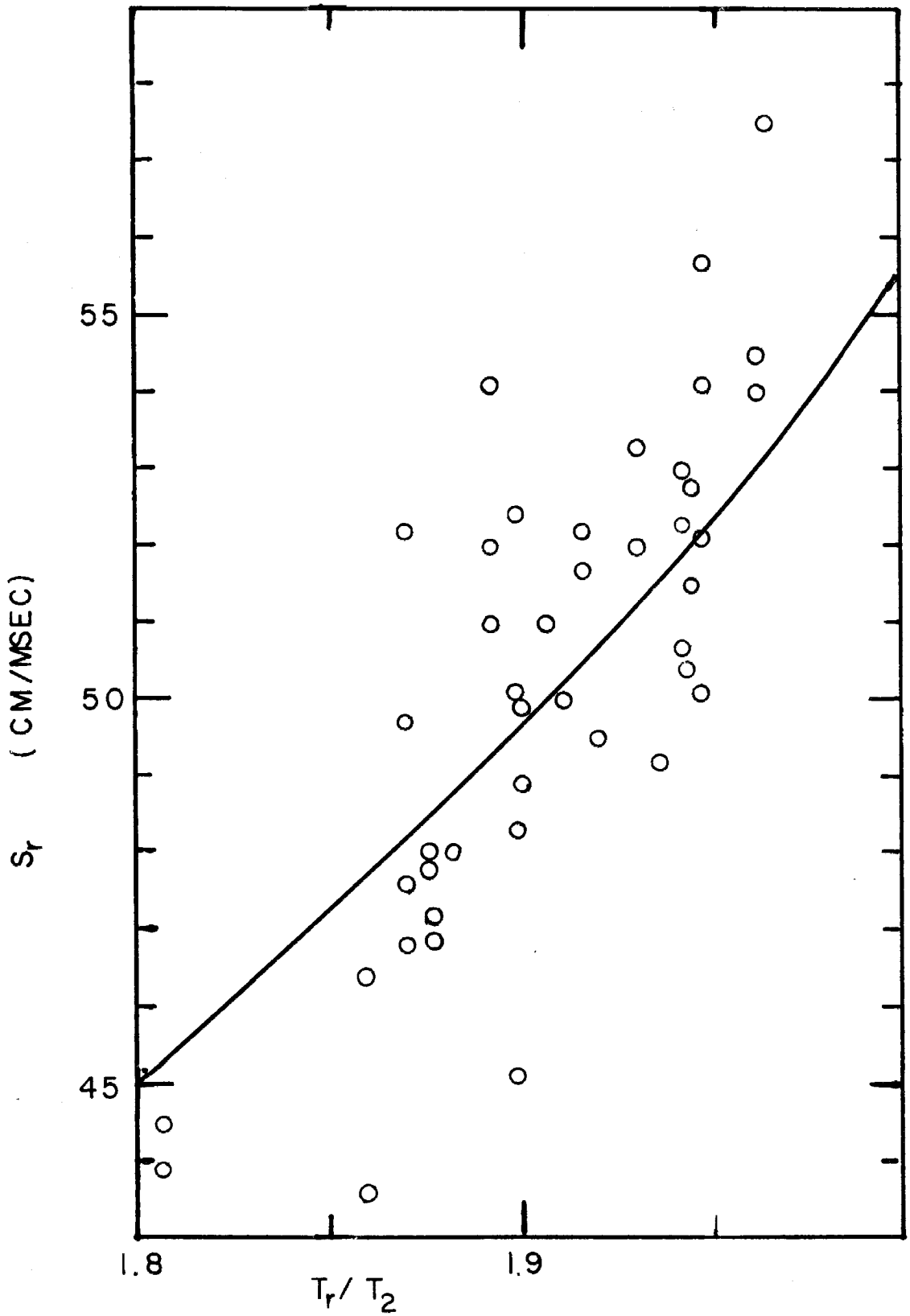

Figure 3. Measured and Calculated Reflected Shock Speeds
Line from incident shock; points from trace

within experimental error under the same conditions in reflected and incident shock waves. A series of experiments was done at an NO_2 mole fraction of 2.3×10^{-2} and an initial pressure of 0.04 atm behind incident shock waves. Another series at essentially the same mole fraction and an initial pressure of around 0.019 atm was done behind reflected shock waves. Since the ratio Δ_r is around 2.1, the concentrations in the two regions were the same. Measured rate constants for these two types of experiment may be compared on an Arrhenius plot in figure 4 and seen to be equal within the experimental error.

7. Calculation of Rate Constants and Extinction Coefficients

Initial rate constants and extinction coefficients were calculated from the observed records of light intensity as a function of time. The ratio of incident intensity I_o to transmitted intensity I_1 may be calculated for a given composition and pressure of gas by the following expression for the initial optical density D_1.

$$\log_{10} \frac{I_o}{I_1} = \epsilon_1 [NO_2]_1 \ell = D_1 \tag{41}$$

The subscript 1 refers to properties of the unshocked gas; ℓ is the length of the light path. Measurement of ϵ_1, the room temperature extinction coefficient, is discussed later in this section. The intensity I_1 may be obtained from the photoelectric record before the gas is shocked, so the incident intensity I_o is known also. Measured light intensity values at various times can then be converted into optical density values, which have the following simple relation to the degree of reaction α.

$$D = \epsilon_2 \Delta[NO_2]_1 (1 - \alpha) \ell \tag{42}$$

The relation between the NO_2 concentration before and after passage of the shock is given by:

$$[NO_2] = [NO_2]_1 \Delta (1 - \alpha) \tag{43}$$

The symbol α, the degree of reaction, is the same as α_2 of the last section. Differentiating 42 yields the expression:

$$\frac{d \ln D}{dt} = \frac{d \ln \epsilon}{dt} + \frac{d \ln \Delta}{dt} - \frac{1}{(1-\alpha)} \frac{d\alpha}{dt} \tag{44}$$

The last term of 44, the chemical reaction term, is much larger than the other two under the usual conditions of a large excess of buffer gas. The expression, 44, may be rearranged to give:

$$\frac{d \ln D}{dt} = \frac{d\alpha}{dt} \left[\frac{d \ln \epsilon}{d \alpha} + \frac{d \ln \Delta}{d \alpha} - \frac{1}{1-\alpha} \right] \tag{45}$$

The particular expression used for $d\alpha/dt$ depends on the assumed mechanism of NO_2 decomposition. The total decrease in NO_2 concentration with time, $-d[NO_2]/dt$, is proportional to the sum of the change due to reaction, measured by α, and the change due to density, measured by Δ. For an assumed mechanism whose rate step is proportional to $[NO_2]$ and $[M]$, the total gas concentration, this relation is:

$$\begin{aligned} \frac{d[NO_2]}{dt} &= \left. \frac{\partial [NO_2]}{\partial t} \right|_{\Delta} + \left. \frac{\partial [NO_2]}{\partial \Delta} \right|_{\alpha} \frac{d\Delta}{dt} \\ &= -k_{1\ obs} [NO_2][M] + \left. \frac{\partial [NO_2]}{\partial \Delta} \right|_{\alpha} \frac{d\Delta}{dt} \end{aligned} \tag{46}$$

The first term on the right of 46 is the conventional isochoric reaction rate. Also, $d[NO_2]/dt$ may be obtained from 43.

$$\frac{d[NO_2]}{dt} = -\Delta[NO_2]_1 \frac{d\alpha}{dt} + [NO_2]_1(1-\alpha) \frac{d\Delta}{dt} \qquad (47)$$

The second terms on the right of 46 and 47 are equal, so the first terms may be set equal and rearranged.

$$\frac{d\alpha}{dt} = k_{1\ obs}\Delta[M]_1(1-\alpha) \qquad (48)$$

The time scale with which observations are made on reacting gases behind an incident shock wave is compressed since the reacting gas before the slit at any time has come from upstream. This means the gas has been heated for a time longer than the time since the shock wave has passed the observation station. The relation between the gas time τ and the laboratory time t is $dt = \Delta\, d\tau$, where Δ is the compression ratio. In order to make the times in the expressions above correspond to times measured on the oscilloscope traces, the above relation is introduced. Behind reflected shocks the gas is at rest, and no such correction is needed. Therefore 48 becomes:

$$\frac{d\alpha}{d\tau} = k_{1\ obs}\Delta^2[M]_1(1-\alpha) \qquad (49)$$

The final expression for $k_{1\ obs}$ is obtained by combining 49 and 45 and letting α approach zero for initial rate constants.

$$k_{1\ obs} = \frac{-\left.\frac{d\ ln D}{d\ \tau}\right|_{\alpha=0}}{\Delta^2[M]_1\left[1-\frac{d\ ln\epsilon}{dT}\ \frac{dT}{d\alpha}-\frac{d\ ln\Delta}{d\ \alpha}\right]} \qquad (50)$$

For each experiment, values of ln D were plotted against τ, and the best initial slope obtained for use in the expression above. If one chooses to initiate the interpretation of the data by assuming that the reaction proceeds exclusively by the bimolecular path, the apparent second order constant, $k_{2\ obs}$, can be calculated as:

$$k_{2\ obs} = k_{1\ obs}\frac{[M]_1}{[NO_2]_1} \qquad (51)$$

The term in brackets in 50 is a correction for change in ϵ and Δ with α. It is rarely less than .85 and is usually much closer to unity. To evaluate this term, it is necessary to know $d\epsilon/dT$, $dT/d\alpha$, and $d\Delta/d\alpha$ for each experiment. The factor $d\epsilon/dT$ is obtained from graphs of ϵ_2 versus T. The change in temperature, $dT/d\alpha$, is obtained from the expression:

$$\left.\frac{\partial T}{\partial \alpha}\right|_S = -\frac{\partial S/\partial \alpha|_T}{\partial S/\partial T|_\alpha} \qquad (52)$$

Shock calculations at $\alpha = 0$ and $\alpha = .5$ give two values of S at a given temperature, from which the numerator may be approximated. The denominator may be found from the empirical relation $T_2 = AS^2 + B$, which may be differentiated to give $\partial S/\partial T|_\alpha = 1/(2SA)$. The change in density, $d\Delta/d\alpha$, can be obtained from twice the calculated densities at $\alpha = 0$ and $\alpha = .5$. The correction factors for various experiments were obtained from graphs of the factors against T_2.

By combining relations for the heat absorbed during the reaction with the hydrodynamic expressions, one can obtain explicit relations for $dT/d\alpha$ and $d\Delta/d\alpha$. Values calculated from these relations agree well with the more approximate values described above for one mixture. Therefore, the approximate corrections are used throughout.

Room temperature extinction coefficients were measured for each filter combination with a photomultiplier and oscilloscope. Filter combinations described above were used. At 405 and 436 mμ using the Osram and Hanovia arcs, respectively, the absorption of a known pressure of NO_2 was measured in a 10 cm cell with corex windows. At 546 mμ with the Hanovia arc the absorption of a known pressure of NO_2-argon mixture in the shock tube was measured. Decadic extinction coefficients at 300°K were 164, 144 and 29 $\underline{M}^{-1}$ cm^{-1} at 405, 436, and 546 mμ, respectively.

High temperature extinction coefficients were calculated from the room temperature value and the initial decrease in

light intensity. The ratio I_o/I_1 is obtained from 41. The ratio I_1/I_2 is obtained from the observed intensity, I_1, before the shock wave arrived at the station and the extrapolated value of the intensity after the gas had reached the high temperature but before any reaction had occurred. The coefficient ϵ_2 at the high temperature is then given by the expression:

$$\epsilon_2 = \frac{\log_{10} (I_o/I_1)(I_1/I_2)}{[NO_2]_1 \Delta_i \ell} \qquad (53)$$

In the experiments with reflected shocks, ϵ_2 and ϵ_r behind the incident and reflected waves is obtained. The expression for ϵ_r is identical with 53 with the substitution of Δ_T for Δ_i and I_r for I_2. The values observed are more reliable when little reaction occurs. For more rapid reactions, the extrapolation to $\alpha = 0$ is long and uncertain.

The extinction coefficient of NO_2 has been measured over the temperature range of this investigation at nominal wave lengths of 405, 436, and 546 $m\mu$. These values are given in Table 4. As previously found (16), the extinction coefficients decrease with temperature at 405 and 436 $m\mu$, but increase at 546.

C. Results and Conclusions

1. Observed Rate Constants

The principal experimental results are values of initial rate constants at various conditions. Ten groups of reactions were done in which the NO_2 concentration, the argon concentration, and the ratio $[M]/[NO_2]$ were widely varied. The approximate conditions of each group of experiments are presented in Table 5. Since Δ changes slowly with shock strength, the concentrations in the shocked gas vary slightly, and exact concentrations for each experiment are given in Table 6. Rate measurements of these reactions were calculated as discussed above in terms of the conventional rate constants defined below.

$$k_{1\ obs} = - \frac{1}{[NO_2][M]} \frac{d[NO_2]}{dt} \tag{54}$$

$$k_{2\ obs} = - \frac{1}{[NO_2]^2} \frac{d[NO_2]}{dt} \tag{55}$$

From Arrhenius plots of the data calculated in this way, several qualitative conclusions may be drawn. The data from experiments at the higher mole fractions of .05, .10 and .15 may be fitted to a straight line when $k_{2\ obs}$ is plotted on an Arrhenius graph (figure 5). The activation energy is 23 ± 4 kcal / mole, which is within the observed

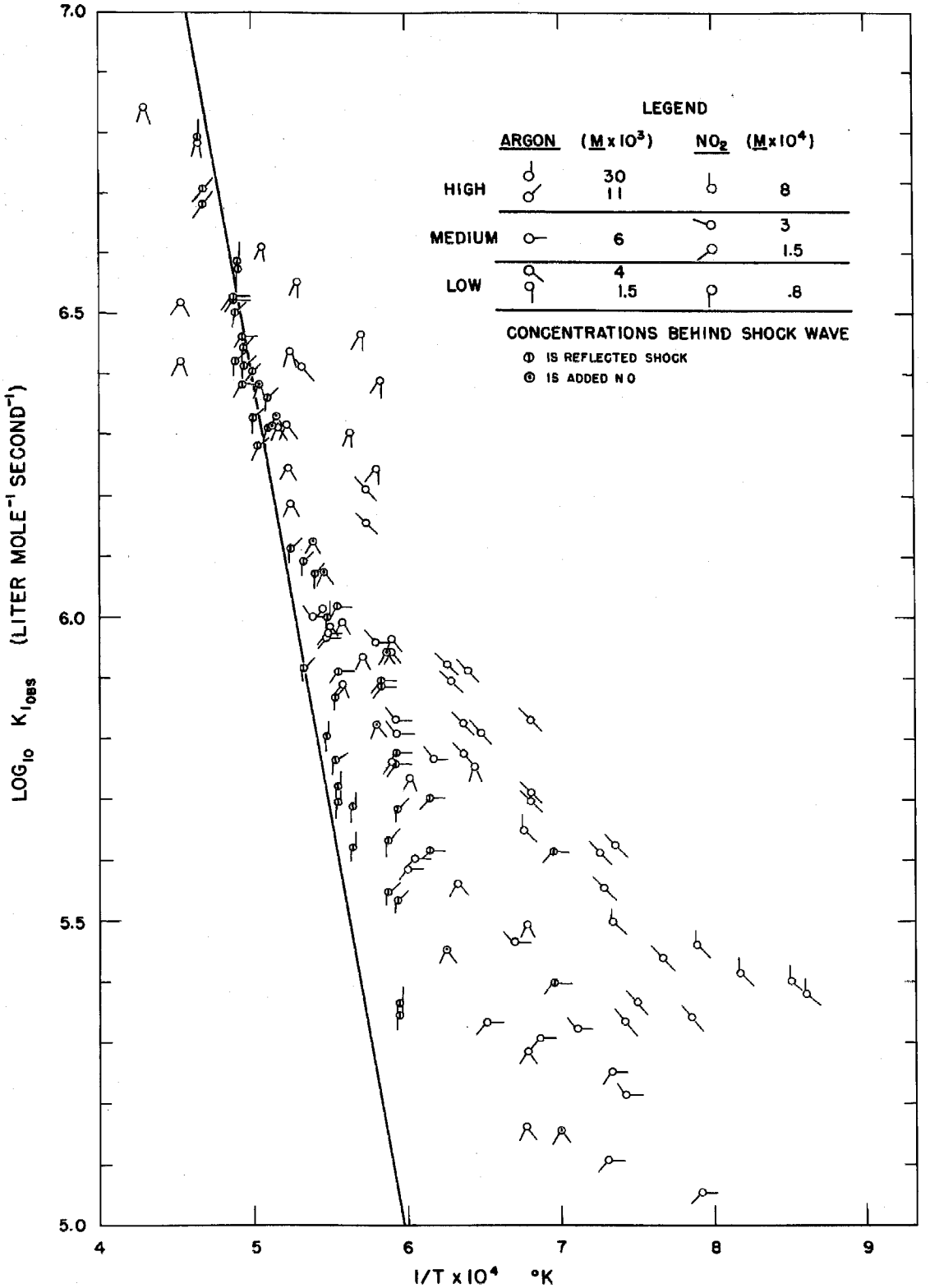

Figure 4

OBSERVED BIMOLECULAR RATE CONSTANTS

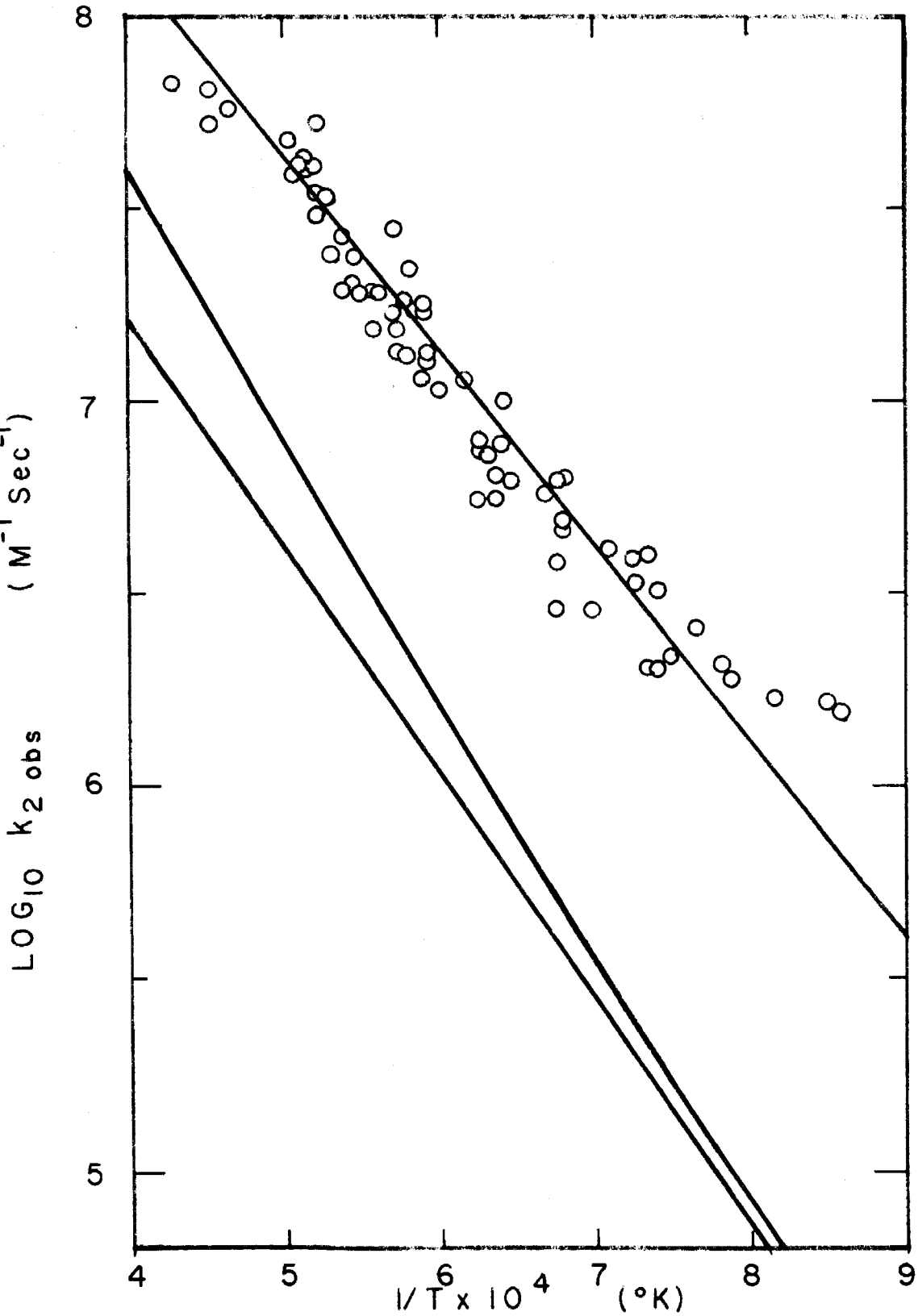

Figure 5. Observed Rate Constants for High NO_2 Concentrations
Lower two lines are extrapolations of low temperature results

Bodenstein activation energy of 26.6 kcal / mole (1). However, the observed rate constants are about twelve times higher than the constants predicted from a straight line extrapolation of the Bodenstein and Ramstetter (1) and Rosser and Wise (5) results to temperatures of this investigation. For example, at 1667°K, $\log_{10} k_{2\ obs}$ is 7.10, while the extrapolated value is 6.03, where the constants are in the units $\underline{M}^{-1}$ sec^{-1}. If data from the four lowest NO_2 mole fraction groups are calculated as $k_{2\ obs}$ and plotted, the results do not fall on the straight line shown in figure 5, but are too high. At 2000°K, the $k_{2\ obs}$ for the lowest NO_2 concentrations are about 12 times higher than the average of the higher concentrations. It is particularly significant that the 2.8×10^{-3} mole fraction mixture rate constants are higher than the 7×10^{-3} mixtures. The NO_2 concentration is the same in both cases, while the argon concentration is three times greater in the latter group. This result suggests a path dependent on the argon or total gas concentration.

The Arrhenius plot of $\log k_{1\ obs}$ (figure 4) seems to apply to all the data much better. In particular, the points of lower NO_2 concentrations near 2000°K seem well established. The highest activation energy observed was 57 kcal/mole for the 2.8×10^{-3} mole fraction points. The points at lower $[M]/[NO_2]$ ratios have lower activation energies, and many groups at higher $[NO_2]$ clearly fall

above the best line through the lower [NO_2] results. Qualitative observations of this sort indicate that more than one process is occurring under these conditions. It should also be pointed out that additions of .043 mole fraction NO to experiments containing .050 mole fraction NO_2 did not affect the rate, as shown in figure 4.

Values of $k_{1\ obs}$ as defined in 54 along with other experimental conditions for each of the ten groups of reactions are given in Table 6.

2. Extrapolation of Proposed Mechanisms

In this section, an attempt will be made to make the best possible extrapolation of reported rate expressions and mechanisms to the conditions of the present experiments.

The detailed extrapolation of the bimolecular NO_2 decomposition observed by Bodenstein and Ramstetter (1) and Rosser and Wise (5) may be carried out using the transition state theory in the manner of Herschbach, Johnston, Pitzer and Powell (4). The rate step for this process is reaction 1 previously given:

$$NO_2 + NO_2 \xrightarrow{k_b} NO + O_2 + NO \qquad (1)$$

The value of k_b over the total range (5) is:

$$k_b = -\frac{1}{[NO_2]^2}\frac{d[NO_2]}{dt} = 4.0 \times 10^9 \exp[-26900/RT]\ \underline{M}^{-1}\text{sec}^{-1} \qquad (56)$$

The extrapolation of these results to temperatures of around 2000°K of this investigation is not accurate unless the detailed temperature dependence of the pre-exponential factor in 56 is known.

Reference 4, hereafter called HJPP, calculates theoretical values of pre-exponential factors for a number of bimolecular gas phase reactions including 1. A detailed form of the

transition state theory is used, which requires all partitions functions of the reactants and the activated complex. Estimates must therefore be made of bond lengths, vibration frequencies, moments of inertia for total and internal rotation, symmetry numbers for the rotations, and ground state electronic degeneracies for the reactants and activated complex. Although in general the pre-exponential factor will vary with temperatures, it is very difficult to observe this variation in any given investigation. Accordingly, an observed pre-exponential factor A, not dependent on temperature has been obtained from the observed rate constant and experimental activation energy, E, at a given temperature from the expression below.

$$A = \frac{k}{\exp\ [-E/RT]} \tag{57}$$

This observed pre-exponential factor may be calculated in terms of the theoretical expression:

$$k = B\ (T)\ \exp\ [-E_o/RT] \tag{58}$$

where B is a function of temperature and E_o is not. The temperature dependent experimental activation energy E in 57 and E_o are related by the expression:

$$E_o = E - RT^2\ \frac{d\ \ln\ B}{dT} \tag{59}$$

An important feature of the method is an approximate method of calculating moments of inertia for internal rotation. For reaction 1, HJPP have assumed a planar activated complex of the form:

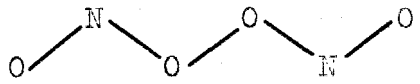

The observed and calculated pre-exponential factors are 1.8×10^9 and 4.5×10^9 $\underline{M}^{-1}$ sec^{-1} at 570°K, using the data of Bodenstein and Ramstetter (1). The recent combined rate expression for the two investigations given by Rosser and Wise has a pre-exponential factor of 4.0×10^9. Either experimental value is in excellent agreement with the theoretical.

Although it would not be a good approximation to use the calculated pre-exponential value for extrapolations, it would be justifiable to use the ratio of the rate constant expression 58 at two temperatures, and the measured rate constant at one temperature, to calculate a rate constant at the upper temperature. This ratio is given by the expression:

$$\frac{k_{T_2}}{k_{T_1}} = \frac{B(T_2)}{B(T_1)} \exp\left[-\frac{E_o}{R}\left(\frac{1}{T_2} - \frac{1}{T_1}\right)\right] \qquad (60)$$

For the transition state theory, B(T) is given by the expression:

$$B(T) = \frac{K k_B T}{h} \frac{Q^{\ddagger}}{Q_A Q_B} \qquad (61)$$

In this expression κ is the transmission coefficient which will be assumed temperature independent, k_b is Boltzmann's constant, h is Planck's constant, $Q^{\ddagger}$ is the partition function for the activated complex with the degree of freedom corresponding to the reaction coordinate removed, and $Q_A Q_B$ are the total partition functions for the reactants. The partition functions are the product of partition functions for translational, electronic, total and internal rotational, and vibrational degrees of freedom. No upper electronic states contribute to the electronic partition function for NO_2 and none are assumed for the complex, so this term in B(T) does not appear in 60. For all other motions except vibration, the high temperature expressions for the partition functions may be considered as a constant times the temperature raised to a certain power. The constants cancel from 60, and one obtains a $T^{-1/2}$ from the temperature dependences. This exponent arises since translation contributes $T^{-3/2}$, total rotation contributes $T^{-3/2}$, internal rotation contributes $T^{3/2}$ and the frequency factor contributes T. Since not all vibrations are excited at all temperatures of this extrapolation, no simple expression holds, and the vibrational partition function Q_v must be calculated at each T_2. With these substitutions, 60 becomes:

$$\frac{k_{T_2}}{k_{T_1}} = \left(\frac{T_1}{T_2}\right)^{1/2} \frac{Q_{v2}}{Q_{v1}} \exp\left[-\frac{E_o}{R}\left(\frac{1}{T_2} - \frac{1}{T_1}\right)\right] \qquad (62)$$

To qualitatively understand the change of k_{T_2} with T_2, a fairly accurate approximation of 62 may be given. The activated complex has been assumed planar, and all vibrations lie in the plane. The six out-of-plane motions include one translation, two total rotations, and three free internal rotations. There are twelve in-plane motions, including two translations, one total rotation, and one reaction coordinate. This leaves eight vibrational frequencies to be estimated. The estimates of six of these are obtained from comparison with the frequencies of NO_2, which are included twice in the denominator of Q_v. The other two motions are low frequency rocking motions of large groups in the complex and give large contributions to the partition function. These estimated frequencies are 350 and 250 cm^{-1}. If the six NO_2 frequencies are allowed to cancel the six largest complex frequencies and the fully excited approximation to the partition function $k_bT/h\nu$ is substituted for the two low frequencies, the expression becomes:

$$\frac{k_{T_2}}{k_{T_1}} = \left(\frac{T_2}{T_1}\right)^{3/2} \exp\left[-\frac{E_o}{R}\left(\frac{1}{T_2} - \frac{1}{T_1}\right)\right] \qquad (63)$$

The Arrhenius plot should therefore show an upward curvature as the temperature increases.

The extrapolation was made from the exact expression, 62, between 570°K, the temperature used by HJPP, and 2500°K using the combined rate constant given by 56. This extra-

polation is shown on figure 5. At 1667°K, E° is found by 59 to be 25.9 kcal/mole compared to 26.9 kcal/mole for E. Moreover, the curve is very sensitive to changes in E_o. The E_o necessary to connect the average shock tube results with 56 at 570°K is 29.3 kcal/mole. While the activation energy is usually not accurately known, this difference of 3.4 kilocalories between the observed value and the value necessary to fit the high temperatures results does seem well outside the experimental uncertainty in the present case. To obtain the same agreement between measured and calculated partition functions at 570°K, the factor B(T) associated with an E_o of 29.3 kilocalories would have to be twenty times greater than the B(T) previously calculated. This factor would seem also somewhat larger than could be obtained by refining the HJPP estimates of parameters. This extrapolation is discussed further in the next section after an analysis of the experimental data obtained in the present work.

Another mechanism giving a rate expression with a quadratic dependence on the NO_2 concentration is the Ashmore and Levitt (6) mechanism shown below, which postulates NO_3 as an unstable intermediate.

$$NO_2 + NO_2 \xrightarrow{k_2} NO_3 + NO \qquad (2)$$

$$NO_3 + NO \xrightarrow{k_3} NO_2 + NO_2 \qquad (3)$$

$$NO_3 + NO_2 \xrightarrow{k_4} NO_2 + O_2 + NO \qquad (4)$$

The rate expression for this mechanism is:

$$-\frac{1}{[NO_2]^2}\frac{d[NO_2]}{dt} = \frac{2\,k_2}{1 + k_3[NO]/k_4[NO_2]}$$

This mechanism is inhibited by NO, either added initially or produced in the reaction, so that it only contributes to the rate during the early stages of the reaction even in pure NO_2. The bimolecular path of reaction 1 is, of course, continuing to occur. At 707°K, Ashmore and Levitt report $k_b = 19.4$, $k_2 = 26$ (both $\underline{M}^{-1}sec^{-1}$) and $k_3/k_4 = 60$. Davidson and Schott (8) give $k_3/k_4 = 570$. Therefore at 707°K, without NO present, initially each path contributes about the same. Both k_3 and k_4 are known from previous kinetics investigation on the nitrogen oxides (7). The values of the pre-exponential factors and the activation energies for k_3 and k_4 are reported as 6×10^{10} and 1.5×10^5 $M^{-1}sec^{-1}$, and 1.4 ± 2.5 and 3.8 ± 1 kcal/mole respectively.

It is difficult to predict whether a mechanism involving NO_3 is important at a temperature of 1750°K, an average for the present investigation. Ashmore and Levitt (8) have some evidence that the activation energy of 2 is 30 kcal/mole. The very small activation energy of 3 given by Schott and Davidson (7) suggests that the activation energy should be ΔH_o° for 2, or 23 kcal/mole. These estimates bracket the observed bimolecular activation energy, 26.9 kcal/mole, so it is possible that k_2 would be comparable with k_b at 1750°K.

Using the activation energies of Schott and Davidson (7), k_3/k_4 would become 20 (AL) or 190 (SD) at 1750°K. If k_3/k_4 were very large, a very small amount of NO would completely inhibit the mechanism. If k_3/k_4 were very small, it might prove impossible at certain temperatures to observe the inhibition in the shock tube even with all the argon replaced by NO. In figure 4 are presented values of $k_{2\ obs}$ for gas mixtures containing .050 mole fraction NO_2 and .043 mole fraction NO in argon. Within the limited precision available, the same rate constants are obtained with and without added NO. Thus, the actual situation is still uncertain.

Another possibility is that a reaction faster than 4 destroys NO_3 at the high temperatures. The unimolecular decomposition of NO_3 at the low pressure limit may be represented by:

$$NO_3 + M \underset{k_r}{\overset{k_d}{\rightleftharpoons}} NO_2 + O + M \qquad (64)$$

The total reaction would then involve 10, the rapid reaction of O and NO_2, as the final step. An estimate of k_d may be made from the known thermodynamic functions of NO_3 (7) and the rate of the reverse reaction, which has recently been measured by Ford and Endow (23). At 298°K, the equilibrium constant for 64, K_c, is 4.5×10^{-31} M. This value may be extrapolated to high temperatures by using the expression

below for equilibrium constants in terms of partition functions, Q.

$$\frac{K_{c_2}}{K_{c_1}} = \left[\left(\frac{Q_{NO_2}Q_O}{Q_{NO_3}}\right)_2 \Big/ \left(\frac{Q_{NO_2}Q_O}{Q_{NO_3}}\right)_1\right] \exp\left[-\frac{\Delta E_o^\circ}{R}\left(\frac{1}{T_2}-\frac{1}{T_1}\right)\right] \quad (65)$$

The rotational temperature dependence will cancel, since there are three rotational degrees of freedom in both NO_3 and NO_2. The six vibrations of NO_3 may be classified as three stretches, two bends, and one out-of-plane vibration. The vibrations of NO_2 consist of two stretches and one bend. If it is assumed that the stretches make small contributions, that one bend may be cancelled in NO_2 and NO_3, and that the other two vibrations of NO_3 are classical, the total contribution from vibrations is T^{-2}. Therefore, 65 may be written:

$$\frac{K_{c_2}}{K_{c_1}} = \left(\frac{T_1}{T_2}\right)^{1/2} \exp\left[-\frac{\Delta E_o^\circ}{R}\left(\frac{1}{T_2}-\frac{1}{T_1}\right)\right] \quad (66)$$

If $\Delta E^\circ_{298} = 49.6$ kcal/mole is used for ΔE_o°, K_c at 1750°K is .29. Ford and Endow report $k_r = 1.0 \times 10^{11}\ \underline{M}^{-2}\ sec^{-1}$ at 298°K. Reactions of this type are expected to have a temperature dependence of approximately T^{-1} to T^{-2}, and in the present case $T^{-3/2}$ was used. Therefore, k_r at 1750°K is $7.0 \times 10^9\ \underline{M}^{-2} sec^{-1}$, and k_d is $2.0 \times 10^9\ \underline{M}^{-1}\ sec^{-1}$.

If 64 replaces 4 in the Ashmore and Levitt mechanism, the rate expression is:

$$-\frac{1}{[NO_2]^2}\frac{d[NO_2]}{dt} = \frac{2\,k_2}{1 + k_3[NO]/k_d[M]} \qquad (67)$$

From the expression given by Schott and Davidson (7), $k_3 = 4 \times 10^{10}\ \underline{M}^{-1}\text{sec}^{-1}$ at 1750°K. Using the values of [NO] and [M] present in the inhibition experiments, one obtains $k_3\,[NO] = 4 \times 10^{6}\ \text{sec}^{-1}$ and $k_d\,[M] = 5 \times 10^{6}\ \text{sec}^{-1}$ or $k_3\,[NO]/k_d[M] \sim 1$. Therefore, 64 may indeed become important at high temperatures. The inhibition by NO would not be observed at temperatures higher than 1750, since k_d has about 50 kcal/mole activation energy, while k_3 has 1.4 kcal/mole. The rate expression 67 would then become identical with the simple bimolecular process and demonstration of this path would be quite difficult in the absence of information from lower temperatures about k_2.

Yet another process which may cause the thermal decomposition of NO_2 at high temperature is the unimolecular decomposition, and the standard mechanism of this type is presented below.

$$NO_2 + M \xrightarrow{k_u} NO_2^* + M \qquad (68)$$

$$NO_2^* + M \longrightarrow NO_2 + M \qquad (69)$$

$$NO_2^* \longrightarrow NO + O \qquad (70)$$

$$O + NO_2 \longrightarrow O_2 + NO \qquad (71)$$

The first three reactions represent the unimolecular decomposition. The last reaction completes the process and

is not rate determining. For a simple triatomic molecule like NO_2, theory and general experience predicts that the rate will depend on the total pressure. In other words, the overall decomposition rate will equal the rate of production of energized NO_2, NO_2^*. This is the same as the rate of 68, or $k_u[NO_2][M]$. In these equations, M represents any gas molecule, and initially this could be either argon or NO_2. The efficiencies of NO_2 and argon in energizing NO_2 are assumed to be equal. An energized NO_2^* molecule contains enough energy to dissociate, but the energy is distributed among several degrees of freedom. When this energy by chance becomes localized in an N-O bond, the molecule breaks into NO and O as shown in 70. If the energized NO_2^* experiences a successful collision with another molecule before this energy becomes localized, the excess energy is lost, and the molecule becomes NO_2 as shown in 69. Since NO_2 is such a simple molecule, the time before the NO_2^* will react is small, and 69 is not effective.

The overall process represented by 68, 69, and 70 may be expressed by 9:

$$NO_2 + M = NO + O + M \qquad (9)$$

The rate of 9 may be estimated from the recent measurements of the rate of the reverse reaction by Ford and Endow (23), an estimation of its temperature coefficient, and the

equilibrium constant of 9. The temperature coefficient of the reverse reaction may be estimated from the temperature dependence of the equilibrium constant and the rate of the forward reaction. The equilibrium constants at two temperatures are related by 65, if $Q_{NC}Q_O/Q_{NO_2}$ is the partition function quotient. Translation contributes $T^{3/2}$, rotation contributes $T^{-1/2}$, and one bending vibration contributes T^{-1} to the temperature dependence. Therefore the quotient has no temperature dependence. The forward unimolecular rate constant may be approximated by:

$$k_u = \frac{Z}{(s-1)!}\left(\frac{E_o}{RT}\right)^{s-1} \exp\left[-\frac{E_o}{RT}\right] \qquad (72)$$

This expression is given by the classical Rice, Ramsperger, Kassel theory, where Z is the collision number and s is the number of effective oscillators--classically 3(number of atoms) minus 6. In the present case s is three and the pre-exponential factor in the above equation has a $T^{-3/2}$ temperature dependence. It is known that the reverse of 9 has little activation energy, so E_o in 72 and ΔE_o° in 65 must be approximately equal. Since the ratio of the forward to the reverse rate constant is the equilibrium constant, the reverse rate constant will have only a $T^{-3/2}$ dependence on the temperature. Arguments of this type justify the temperature dependence assumed for the reverse of 64 above.

Ford and Endow give the rate constant for the reverse

of 9 as 1.8×10^{10} $\underline{M}^{-2}sec^{-1}$ at 300°K with N_2 as the "third body" M. Assuming that argon is about one-half as effective as N_2, the constant becomes 1.0×10^{10} $\underline{M}^{-2}sec^{-1}$. Using the $T^{-3/2}$ temperature dependence derived above, the rate constant is 4.1×10^{8} and 5.8×10^{8} $\underline{M}^{-2}sec^{-1}$ at 2500 and 2000°K, respectively. The equilibrium constant for 9, $[NO][O]/[NO_2]$, may be calculated from standard thermodynamic information (20), (21), (22). It is found to be 3.83×10^{-2} $\underline{M}$ and 1.15×10^{-3} $\underline{M}$ at 2500 and 2000°K, respectively. Therefore the rate constants k_u are 3.2×10^{7} and 1.3×10^{6} $\underline{M}^{-1}sec^{-1}$ at 2500 and 2000°K, where the values calculated as indicated above have been multiplied by two because $k_{1\ obs}$ has been defined, 54, for the decomposition of two NO_2 molecules per reaction. The values of $k_{1\ obs}$ at 2500 and 2000°K are 4.4×10^{7} and 2.6×10^{6} $\underline{M}^{-1}sec^{-1}$ in good agreement with the extrapolation. Therefore, it is not unreasonable to assume that the rate constants measured at the higher temperatures of this investigation are due mainly to a unimolecular reaction.

The local activation energy of the unimolecular reaction 9 may be estimated from the $T^{-3/2}$ temperature dependence of the pre-exponential factor. The energy E_o in 76 is taken as ΔH_o° of reaction 9 or 71.381 kcal/mole (22). The predicted local activation energy, E, is given by 59. In the present case 59 becomes $E = E_o - (3/2)RT$, and therefore around 2000°K, E is 65.4 kcal/mole. This estimate will be used in the analysis of the rate data to be presented in the next section.

3. Interpretations and Comparisons

This section will describe an analysis of the observed rate constants that indicates the Bodenstein bimolecular decomposition and a unimolecular process are both occurring. Also, the results of this investigation will be compared with the results of the Steinburg and Lyon (9) investigation.

The analysis of observed rate constants into a bimolecular contribution k_b and a unimolecular contribution k_u was accomplished by subtracting an estimated value of k_u from the observed rate constant $k_{1\ obs}$ (figure 4). The estimation of the local activation energy E to be 65.4 kcal/mole around 2000°K was discussed in the last section. Since one value of k_u must be known in addition to the local activation energy, it was judged most reasonable to draw several lines of 65.4 kcal/mole activation energy, and compare the k_b values obtained. These lines were drawn almost through the results for low NO_2 concentrations at around 2000°K. The bimolecular rate constant was determined from the expression:

$$k_b = \frac{[M]_1}{[NO_2]_1}\left[k_{1\ obs} - k_u\right] \qquad (73)$$

The best rate expression found was $k_u = 3.06 \times 10^{13} \exp [-65400/RT]\ \underline{M}^{-1}\text{sec}^{-1}$, and it is shown in figure 4. The large slope of this line means that the rate constants are greatly affected at high temperatures and not changed at all at lower temperatures by this analysis. The Arrhenius plot

of log k_b, determined by 73, versus reciprocal temperature is shown in figure 6. As might be expected, the scatter at the higher temperatures is much greater than at the low temperatures. However, the significant point is that the groups with low NO_2 mole fractions of 2.8×10^{-3}, 7×10^{-3} and 2.3×10^{-2} are now much better represented on a single line. The experimental activation energy of figure 6 is 22 ± 6 kcal/mole. Comparison of figure 5 and figure 6 show that the higher NO_2 concentration results are not affected much. The extrapolation of the bimolecular path using experimentally determined quantities and the transition state theory is still almost eight times too low. Also, the extrapolated and observed values are in poor agreement at low temperatures.

The agreement between observed and extrapolated k_b values might be improved if more information were available about the Ashmore and Levitt mechanism (6). At the present time, values have only been published for one temperature. The activation energy of 2 is needed, and measurements of the unimolecular decomposition of NO_3 might prove very significant. Because only one set of NO inhibition experiments were performed and because the extrapolation of k_3/k_4 is quite uncertain, the inhibition experiments should not be interpreted as ruling out the Ashmore and Levitt mechanism. Experiments with a small amount of NO_2 in NO as the buffer gas between 1100 and 1500°K would give probably

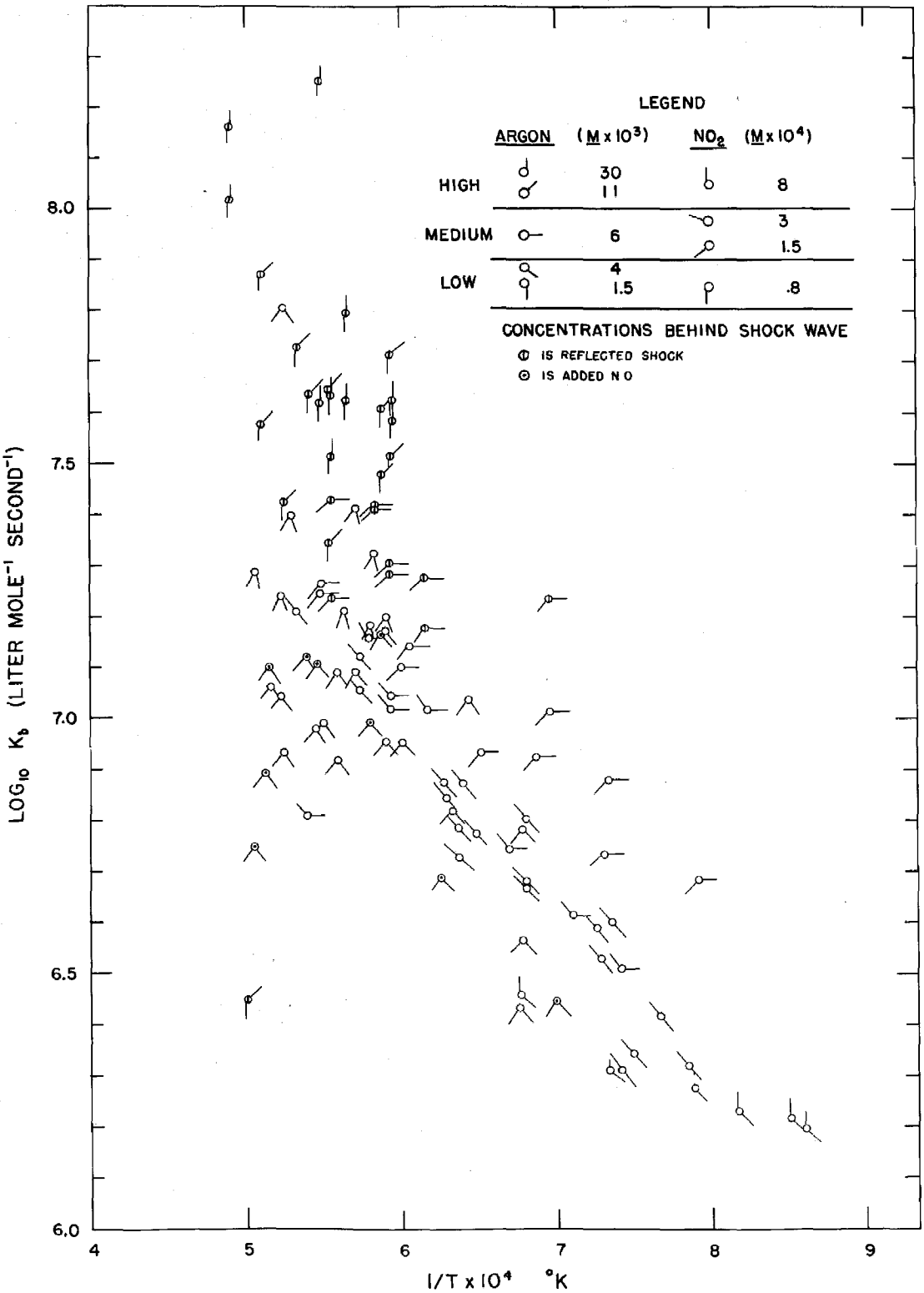

Figure 6

CALCULATED BIMOLECULAR RATE CONSTANT

the greatest chance of observing inhibition by NO.

As previously noted, the results of Steinburg and Lyon (9) on the same system over the same temperature range are somewhat different. They find all their data may be accounted for by the rate expression:

$$k_{SL} = -\frac{1}{[NO_2][A]}\frac{d[NO_2]}{dt}$$

$$= 3.82 \times 10^{11} \exp\,[-46100/RT]\ \underline{M}^{-1}\text{sec}^{-1} \qquad (74)$$

Near 2000°K the results are in agreement. The expression above gives $k_{SL} = 3.4 \times 10^{6}\ \underline{M}^{-1}\text{sec}^{-1}$. At lower temperatures, the larger NO_2 concentration experiments definitely fall above the Steinburg and Lyon expression. Values of k_{SL} were obtained from an integrated form of 74. In the present investigation it was felt that density and temperature changes, with the resultant changes in the rate constant and extinction coefficient, would make integrated expressions less certain than initial expressions. These objections are admittedly less important at low NO_2 mole fractions of .01 to .03 used by Steinburg and Lyon.

The following mechanism was proposed by Steinburg and Lyon.

$$NO_2 + A \xrightarrow{k_5} NO_2^* + A \qquad (5)$$

$$NO_2^* + A \xrightarrow{k_6} NO + O + A \qquad (6)$$

$$NO_2^* + A \xrightarrow{k_7} NO_2 + A + h\nu \qquad (7)$$

$$NO_2 + O \xrightarrow{k_8} NO + O_2 \qquad (8)$$

If NO_2^* and O are present in steady state concentrations and k_6 k_7, the mechanism above gives the concentration dependence of 74. The experimental justification for 7 is stated to be the fact that the light intensity is proportional to the product $[NO_2][A]$. Since an activation energy of 46 kcal/mole is observed, it is believed that 9--which requires about 71 kcal/mole--is not occurring.

The Steinburg and Lyon mechanism is difficult to justify physically. Since about 71 kcal/mole must be involved in going from the reactants of 5 to the products of 6, reaction 6 must have an activation energy of at least 25 kcal/mole if 5 has a 46 kcal/mole activation energy. This additional energy comes from another collision with argon, as shown in reaction 6. It must be postulated that the collision is much more likely to give 25 kcal/mole more energy to the NO_2^* than it is to remove the excess 46 kcal/mole present in the molecule, i.e. to reverse 5. This possibility seems unlikely from previous experience.

The observation of a single activation energy equal to 46 kcal/mole is not supported by the present experiments. Steinburg and Lyon investigated the reaction over an [argon]/$[NO_2]$ ratio of three and an argon pressure ratio of

two. The present study included their conditions but with ranges of sixty-five and twenty for the above quantities. It is clear that the observed activation energy changes with conditions, and in experiments designed to favor the unimolecular process, a measured activation energy of 57 kcal/mole was observed in this study. The results presented here would indicate that both the bimolecular and unimolecular processes were occurring in the Steinburg and Lyon experiments, and therefore an activation energy intermediate between 25.9 and 71 kcal/mole would be observed.

In summary, then, it is believed that the most reasonable interpretation of the shock tube experiments, taking into account the experimental data, extrapolation of other results, and general theoretical considerations, is that NO_2 is decomposing by two paths. One is the unimolecular decomposition of NO_2 into NO and O with a rate law $- d[NO_2]/dt = k_u[NO_2][M]$, and an activation energy of about 65 kcal/mole. The second is a bimolecular decomposition, $- d[NO_2]/dt = k[NO_2]^2$, with an activation energy of 22 ± 6 kcal/mole. However, the limited precision of the shock tube work makes it impossible to definitely prove that the above interpretations are correct.

The observed bimolecular rate constants are greater by a factor of eight than extrapolated values for the bimolecular Bodenstein mechanism. It seems unlikely, but not entirely excluded, that this is due to an error in the

extrapolation. Possibly the Ashmore and Levitt mechanism, or a simple extension thereof (including reaction 64), can account for the additional reaction path. Possibly there is some other as yet unrecognized reaction path. Possibly the discrepancy is in the present work. This question requires further work, but the present investigation has fairly definitely established the occurrence of both unimolecular and bimolecular reaction paths.

D. Tables

Table 1. Gas Parameters for Argon behind Reflected Shock Waves

$T_1 = 300.00^{\circ}K$; Data for incident shocks taken from reference (19)

$\frac{S_i}{a_i}$	Π_i	Δ_i	S_i (cm/msec)	T_2 ($^{\circ}K$)
1.80	3.80000	2.07692	58.059	548.9
2.00	4.75000	2.28571	64.510	623.4
2.20	5.80000	2.46939	70.961	704.6
2.40	6.95000	2.63014	77.412	792.7
2.60	8.20000	2.77049	83.863	887.9
2.80	9.55000	2.89299	90.314	990.3
3.00	11.00000	3.00000	96.765	1100.0
3.20	12.55000	3.09366	103.216	1217.0
3.40	14.20000	3.17582	109.667	1341.4

S_r (cm/msec)	Δ_r	θ_r	Δ_t	T_r ($^{\circ}K$)
37.989	1.79245	1.55925	3.72278	855.9
40.319	1.90000	1.65414	4.34285	1031.3
42.811	1.98630	1.73638	4.90495	1223.5
45.426	2.05621	1.80764	5.40812	1433.0
48.134	2.11340	1.86941	5.85515	1659.9
50.917	2.16063	1.92304	6.25068	1904.4
53.758	2.20000	1.96970	6.60000	2166.7
56.648	2.23310	2.01040	6.90845	2446.7
59.577	2.26115	2.04603	7.18101	2744.5

Table 2. Gas Parameters behind Incident Shocks for Mixtures of Nitrogen Oxides and Argon

T_1 = 300.00°K; Calculations made for first sample of a given composition; Other samples within 1%

Mole Fraction NO_2 = 5.03 x 10^{-2}; Initial pressure = 0.02 atm

T_2 (°K)	π_i	Δ_i	S_i (cm/msec)
	α_2 = 0		
1000	10.395	3.1185	92.55
1500	17.705	3.5410	120.1
2000	25.082	3.7623	142.6
2500	32.482	3.8979	162.0
	α_2 = 0.50		
1000	11.4977	3.4063	95.96
1500	18.7861	3.7106	122.8
2000	26.1487	3.8699	145.0
2500	33.4989	3.9700	164.1

Mole Fraction NO_2 = 5.03 x 10^{-2}; Initial pressure = 0.04 atm

T_2 (°K)	π_i	Δ_i	S_i (cm/msec)
	α_2 = 0		
1000	10.412	3.1240	92.62
1500	17.721	3.5436	120.2
2000	25.095	3.7636	142.6
2500	32.497	3.8997	162.0
	α_2 = .50		
1000	11.5137	3.4111	96.01
1500	18.8023	3.7136	122.9
2000	26.1647	3.8758	145.0
2500	33.5151	3.9717	164.1

Table 2. (continued)

Mole Fraction NO_2 = 1.068 x 10^{-1}; Initial pressure = 0.02 atm

T_2 (°K)	π_i	Δ_i	S_i (cm/msec)
	$\alpha_2 = 0$		
1000	11.2453	3.3738	94.60
1500	19.3202	3.8640	123.2
2000	27.5077	4.1254	146.6
2500	35.7466	4.2900	166.9
	$\alpha_2 = 0.50$		
1000	13.5908	3.9709	101.7
1500	21.6126	4.2101	128.9
2000	29.7281	4.3432	151.4
2500	37.8961	4.4290	171.1

Mole Fraction NO_2 = 1.068 x 10^{-1}; Initial pressure = .010 atm

T_2 (°K)	π_i	Δ_i	S_i (cm/msec)
	$\alpha_2 = 0$		
1000	11.2098	3.3630	94.49
1500	19.2843	3.8569	123.15
2000	27.4716	4.1208	146.6
2500	35.7105	4.2854	166.8
	$\alpha_2 = 0.50$		
1000	13.5551	3.9608	101.6
1500	21.5766	4.2032	128.8
2000	29.6920	4.3380	151.4
2500	37.8599	4.4251	171.0

Table 2. (continued)

Mole Fraction NO_2 = 2.35 x 10^{-2}; Initial pressure = 0.04 atm

T_2 (°K)	π_i	Δ_i	S_i (cm/msec)
	$\alpha_2 = 0$		
600	4.5639	2.2821	62.83
1000	10.0117	3.0035	91.69
1500	16.9586	3.3917	118.7
2000	23.9972	3.5920	140.7
2500	30.9524	3.7145	159.7
	$\alpha_2 = 0.50$		
600	5.0579	2.5141	64.75
1000	10.5222	3.1382	93.26
1500	17.4593	3.4714	119.9
2000	24.4324	3.6433	141.8
2500	31.4218	3.7485	160.7

Mole Fraction NO_2 = 1.527 x 10^{-1}; Initial pressure = 0.03 atm

T (°K)	π_i	Δ_i	S_i (cm/msec)
	$\alpha_2 = 0$		
900	10.2992	3.4331	89.53
1200	15.4555	3.8639	109.10
1500	20.7015	4.1404	125.9
	$\alpha_2 = 0.50$		
900	13.7356	4.4101	100.26
1200	18.8744	4.5450	118.26
1500	24.0852	4.6399	134.02

Table 2. (continued)

Mole Fraction NO = 4.30×10^{-2}; Initial pressure = 0.020 atm
Mole Fraction NO_2 = 5.00×10^{-2}

T_2 (°K)	π_i	Δ_i	S_i (cm/msec)
	$\alpha_2 = 0$		
1000	10.650	3.1950	93.30
1500	18.207	3.6413	121.2
2000	25.850	3.8774	144.1
2500	33.529	4.0234	163.8
	$\alpha_2 = 0.50$		
1000	11.7448	3.4800	96.66
1500	19.2739	3.8072	123.9
2000	26.8983	3.9849	146.4
2500	34.5232	4.0917	165.8

Table 3. Measured and Calculated Reflected Shock Speeds

Mole Fraction $NO_2 = 2.38 \times 10^{-2}$; Initial pressure = .04 atm

Experiment and Scope	Reflected Wave Speed S_r (cm/msec) From S_i	From trace	Θ_r
129-1	49.7	48.9	1.900
129-2	"	49.9	"
130-1	48.4	48.0	1.872
130-2	"	48.8	"
131-1	48.8	46.9	1.877
131-2	"	47.2	"
132-1	52.3	50.5	1.943
132-2	"	50.4	"
133-1	45.5	43.9	1.807
133-2	"	44.5	"
134-1	47.7	43.6	1.860
134-2	"	46.4	"
135-1	52.4	52.1	1.947
135-2	"	50.1	"

Table 3. (continued)

Mole Fraction NO_2 = 7.12 x 10^{-3}; Initial pressure = .04 atm

Experiment and Scope	Reflected Wave Speed S_r From S_i (cm/msec)	From trace (cm/msec)	θ_r
115-1	48.4	46.8	1.870
115-2	"	47.6	"
108-1	48.6	48.0	1.876
108-2	"	47.8	"
113-1	49.8	45.1	1.899
113-2	"	48.3	"
97-1	50.3	50.0	1.911
114-1	50.6	52.2	1.916
114-2	"	51.7	"
98-2	51.0	49.5	1.920
105-1	51.5	52.0	1.930
105-2	"	53.3	"
104-1	51.8	49.2	1.936
109-1	52.2	53.0	1.942
109-2	"	50.7	"
112-1	52.2	52.3	1.942
112-2	"	51.9	"
107-1	52.4	51.5	1.944
107-2	"	52.8	"
110-1	53.4	54.0	1.961
110-2	"	54.5	"
100-2	55.9	54.7	2.003

Table 3. (continued)

Mole Fraction NO_2 = 2.8 x 10^{-3}; Initial pressure = 0.1 atm

Experiment and Scope	Reflected Wave Speed S_r From S_i (cm/msec)	Reflected Wave Speed S_r From trace (cm/msec)	Θ_r
127-1	50.1	54.2	1.907
127-2	"	51.0	"
128-1	53.5	57.5	1.963
136-1	49.5	51.0	1.892
136-2	"	52.0	"
137-1	48.3	49.7	1.870
137-2	"	52.2	"
138-1	52.3	55.7	1.947
138-2	"	54.1	"
139-1	49.8	50.1	1.898
139-2	"	52.4	"

Table 4. High Temperature Extinction Coefficients of NO_2

$\lambda = 436$ mμ; $\epsilon = 144 M^{-1}cm^{-1}$ at 300°K

Experiment and Scope	T_r (°K)	ϵ_r ($M^{-1}cm^{-1}$)	T_2 (°K)	ϵ_2 ($M^{-1}cm^{-1}$)
Mole Fraction NO_2 = 2.8 x 10^{-3}; Initial pressure = 0.10 atm				
127-1	1829	89	959	109
127-2	"	108	"	109
128-1	2150	113	1095	113
136-1	1775	94	938	107
136-2	"	108	"	107
137-1	1682	98	899	114
137-2	"	100	"	115
138-1	2040	145	1048	112
138-2	"	141	"	110
139-1	1800	112	948	112
139-2	"	117	"	110
Mole Fraction NO_2 = 7.12 x 10^{-3}; Initial pressure = 0.04 atm				
106-2	1300	110	737	119
106-1	"	118	"	118
115-1	1687	97	902	117
115-2	"	104	"	118
108-1	1703	92	907	113
108-2	"	99	"	117
113-1	1808	88	952	110
113-2	"	91	"	116
97-1	1848	91	967	106
114-2	1878	93	980	114
114-1	"	87	"	111
98-2	1907	99	993	110
105-2	1961	100	1016	105
105-1	"	88	"	102
104-1	1988	76	1027	103
109-2	2018	78	1039	110
109-1	"	75	"	107

Table 4. (continued)

Experiment and Scope	T_r (°K)	ϵ_r ($\underline{M}^{-1}cm^{-1}$)	T_2 (°K)	ϵ_2 ($\underline{M}^{-1}cm^{-1}$)
112-1	2025	89	1043	110
112-2	"	102	"	113
107-2	2047	97	1053	113
107-1	"	81	"	110
110-2	2138	81	1090	112
110-1	"	70	"	110
100-2	2388	134	1192	81
Mole Fraction NO_2 = 2.38 x 10^{-2}; Initial pressure 0.019 atm				
129-2	1809	104	952	120
129-1	"	97	"	115
130-2	1689	102	902	121
130-1	"	104	"	120
131-2	1716	106	913	123
131-1	"	104	"	119
132-2	2030	84	1045	110
132-1	"	86	"	113
133-2	1439	113	796	125
133-1	"	107	"	120
134-2	1630	107	876	124
134-1	"	104	"	118
135-2	2048	94	1052	115
135-1	"	94	"	112

Table 4. (continued)

Experiment and Scope	T_2 (°K)	ϵ_2 ($\underline{M}^{-1}cm^{-1}$)	Experiment and Scope	T_2 (°K)	ϵ_2 ($\underline{M}^{-1}cm^{-1}$)
Mole Fraction NO_2 = 2.34 x 10^{-2}; Initial pressure = 0.04 atm					
68-2	1262	105	93-2	1366	109
70-2	1828	80	94-2	1652	96
71-2	1667	87	95-2	1827	85
72-2	1370	102	96-2	1459	103
92-2	1535	98			
Mole Fraction NO_2 = 5.04 x 10^{-2}; Initial pressure = 0.02 atm					
2-1	1520	99	13-1	1916	84
3-1	1580	102	14-1	1750	90
6-1	1910	79	17-1	2209	87
10-1	1477	100	21-1	1790	93
11-1	1694	94			
Mole Fraction NO_2 = 5.00 x 10^{-2}; Initial pressure = 0.02 atm Mole Fraction NO = 4.30 x 10^{-2}					
117-2	1726	95	123-2	1707	95
118-2	1830	87	124-2	1858	88
119-2	1985	74	125-2	1952	73
121-2	1598	101	126-2	1942	77
122-2	1431	104			
Mole Fraction NO_2 = 5.09 x 10^{-2}; Initial pressure = 0.04 atm					
34-1	1727	91	37-1	1497	61
35-1	1621	96	38-1	1858	85
36-1	1689	91			
Mole Fraction NO_2 = 1.05 x 10^{-1}; Initial pressure = 0.01 atm					
76-2	2324	51	82-2	1719	91
77-2	2150	74	84-2	1777	91
79-2	1726	89	90-2	1890	83
81-2	1750	93	91-2	1976	86

Table 4. (continued)

Experiment and Scope	T_2 (°K)	ϵ_2 ($\underline{M}^{-1}cm^{-1}$)	Experiment and Scope	T_2 (°K)	ϵ_2 ($\underline{M}^{-1}cm^{-1}$)
Mole Fraction NO_2 = 1.06×10^{-1}; Initial pressure = 0.02 atm					
43-1	1471	99	52-2	1564	102
44-1	1570	96	53-2	1748	91
45-1	1143	108	54-2	1748	94
46-1	1335	103	55-2	1544	102
47-2	1471	100	57-2	1303	102
48-2	1598	95	58-2	1349	104
49-2	1277	107	59-2	1375	103
50-2	1591	96	60-2	1379	106
51-2	1360	107	89-2	1880	79

$\lambda = 405$ mμ; $\epsilon = 164\ \underline{M}^{-1}cm^{-1}$ at 300°K

Experiment and Scope	T_2 (°K)	ϵ_2 ($\underline{M}^{-1}cm^{-1}$)	Experiment and Scope	T_2 (°K)	ϵ_2 ($\underline{M}^{-1}cm^{-1}$)
Mole Fraction NO_2 = 5.04×10^{-2}; Initial pressure = 0.02 atm					
3-2	1580	114	24-2	1478	116
4-2	1660	110	25-2	1936	90
6-2	1910	121	26-2	1558	115
10-2	1477	117	27-2	1695	103
11-2	1694	106	28-2	1832	97
13-2	1916	93	29-2	1818	97
17-2	2209	87	1-2	894	130
21-2	1790	104			

Table 4. (continued)

Experiment and Scope	T_2 (°K)	ϵ_2 ($\underline{M}^{-1}cm^{-1}$)	Experiment and Scope	T_2 (°K)	ϵ_2 ($\underline{M}^{-1}cm^{-1}$)
Mole Fraction NO_2 = 5.09×10^{-2}; Initial pressure = 0.04 atm					
31-2	1349	123	39-2	1234	123
32-2	1408	125	40-2	1234	183
36-2	1689	106			
Mole Fraction NO_2 = 1.06×10^{-2}; Initial pressure = 0.02 atm					
41-2	1172	125	44-2	1570	106
43-2	1471	111	45-2	1143	126

λ = 546 mμ; ϵ = 29 $\underline{M}^{-1}cm^{-1}$ at 300°K

Experiment and Scope	T_2 (°K)	ϵ_2 ($\underline{M}^{-1}cm^{-1}$)	Experiment and Scope	T_2 (°K)	ϵ_2 ($\underline{M}^{-1}cm^{-1}$)
146-2	1053	56	150-2	1269	62
147-2	1224	63	151-2	1162	55
148-2	1364	60	152-2	1176	57
149-2	1478	60			

Table 5. Range of Experimental Conditions

$\frac{[M]}{[NO_2]}$	Unshocked gas		Shocked gas		Wave region
	Mole Fraction NO_2 ($\times 10^2$)	Pressure (atm)	$[NO_2]$ ($\underline{M} \times 10^4$)	$[A]$ ($\underline{M} \times 10^3$)	
357	0.28	0.1	.8	30	reflected
143	0.7	0.04	.8	11	"
44	2.3	0.019	1.5	6	"
44	2.3	0.04	1.5	6	incident
20	5.0	0.02	1.5	3	"
20	5.0	0.02	1.5	3	" (NO)
20	5.0	0.04	3	6	"
10	10	0.01	1.5	1.5	"
10	10	0.02	3	3	"
6.7	15	0.03	8	4	"

Table 6. Observed Initial Rate Constants

Experiment and Scope	T_2 (°K)	$[NO_2]_1 \Delta$ (M x 10^5)	log $k_{1\ obs}$ (M^{-1} sec^{-1})
Reflected shocks Mole fraction NO_2 = 2.66 x 10^{-3}; Initial pressure = 0.10 atm			
127-2	1829	6.80	6.000
127-1	"	"	5.803
128-1	2150	7.19	6.791
Reflected shocks Mole fraction NO_2 = 2.98 x 10^{-3}; Initial pressure = 0.10 atm			
136-2	1775	7.46	5.622
136-1	"	"	5.690
137-2	1682	7.23	5.348
137-1	"	"	5.368
138-2	2040	7.80	6.588
138-1	"	"	6.576
139-2	1800	7.58	5.722
139-1	"	"	5.696
Reflected shocks Mole fraction NO_2 = 7.12 x 10^{-3}; Initial pressure = 0.04 atm			
115-2	1687	7.07	5.682
115-1	"	"	5.537
108-2	1703	7.04	5.634
108-1	"	"	5.548
113-2	1808	7.12	5.765
113-1	"	"	5.869
97-1	1848	7.24	6.070
114-1	1878	7.23	5.917
114-2	"	"	6.093
98-2	1907	7.44	6.114
105-1	1961	7.62	6.311
105-2	"	"	6.362
104-1	1988	7.94	6.283
109-1	2018	7.73	6.396
109-2	"	"	6.329
112-2	2025	7.67	6.447
112-1	"	"	6.412
107-1	2047	7.98	6.422
107-2	"	"	6.501
110-1	2138	7.67	6.681
110-2	"	"	6.709
100-2	2388	7.76	7.470

Table 6. (continued)

Experiment and Scope	T_2 (°K)	$[NO_2]_1 \Delta$ ($\underline{M} \times 10^4$)	log $k_{1\,obs}$ ($\underline{M}^{-1}$ sec^{-1})
Reflected shocks			
Mole fraction $NO_2 = 2.38 \times 10^{-2}$;		Initial pressure = 0.019 atm	
129-2	1809	1.17	6.019
129-1	"	"	5.911
130-2	1689	1.07	5.759
130-1	"	"	5.777
131-2	1716	1.15	5.887
131-1	"	"	5.893
132-2	2030	1.16	6.463
132-1	"	"	6.381
133-2	1439	1.00	5.615
133-1	"	"	5.399
134-2	1630	1.11	5.701
134-1	"	"	5.618
135-2	2048	1.18	6.523
135-1	"	"	6.526
Mole fraction $NO_2 = 2.34 \times 10^{-2}$;		Initial pressure = 0.040 atm	
68-2	1262	1.25	5.051
92-2	1535	1.32	5.337
71-2	1667	1.33	5.587
72-2	1370	1.28	5.107
70-2	1828	1.38	5.969
93-2	1366	1.28	5.251
94-2	1652	1.38	5.601
95-2	1827	1.35	5.971
96-2	1459	1.32	5.307
Mole fraction $NO_2 = 5.04 \times 10^{-2}$;		Initial pressure = 0.02 atm	
3-2	1580	1.47	5.562
4-2	1660	3.51	5.732
6-2	1910	1.65	6.436
6-1	"	"	6.190
10-2	1477	1.55	5.494
10-1	"	"	5.284
11-2	1694	1.46	5.966
11-1	"	"	5.762
13-2	1916	1.53	6.318
13-1	"	"	6.246

Table 6. (continued)

Experiment and Scope	T_2 (°K)	$[NO_2]_1 \Delta$ ($\underline{M} \times 10^4$)	log $k_{1\ obs}$ ($\underline{M}^{-1}\ sec^{-1}$)
14-1	1750	1.49	5.935
17-2	2209	1.63	6.420
17-1	"	"	6.518
21-1	1790	1.71	5.992
21-2	"	"	5.890
24-2	1478	1.50	5.162
25-2	1936	1.65	6.313
26-2	1558	1.49	5.755
27-2	1695	1.53	5.942
28-2	1832	1.54	6.016
29-2	1818	1.67	5.984
Mole fraction NO_2 = 5.09×10^{-2}; Initial pressure = 0.04 atm			
31-2	1349	3.66	5.215
32-2	1408	3.17	5.323
34-1	1727	3.01	5.959
35-1	1621	3.02	5.767
36-2	1689	2.96	5.831
36-1	"	"	5.807
37-1	1497	2.94	5.469
38-1	1858	3.12	6.001
Mole fraction NO_2 = 5.00×10^{-2}; Initial pressure = 0.02 atm " " NO^2 = 4.30×10^{-2}			
117-2	1726	1.56	5.823
118-2	1830	1.62	6.074
119-2	1985	1.57	6.383
121-2	1598	1.55	5.453
122-2	1431	1.64	5.157
123-2	1707	1.62	5.942
124-2	1858	1.61	6.127
125-2	1952	1.65	6.316
126-2	1942	1.64	6.331
Mole fraction NO_2 = 1.046×10^{-1}; Initial pressure = 0.01 atm			
76-2	2324	1.77	6.843
77-2	2150	1.81	6.781
79-2	1726	1.70	6.246
81-2	1750	1.62	6.468
82-2	1719	1.80	6.372

Table 6. (continued)

Experiment and Scope	T_2 (°K)	$[NO_2]_1 \Delta$ (M x 10^4)	log $k_{1\ obs}$ (M^{-1} sec^{-1})
84-2	1777	1.76	6.302
90-2	1890	1.64	6.552
91-2	1976	1.79	6.611
Mole fraction NO_2 = 1.060 x 10^{-1}; Initial pressure = 0.02 atm			
43-2	1471	3.21	5.712
43-1	"	"	5.698
44-2	1570	3.26	5.829
44-1	"	"	5.775
46-1	1335	3.40	5.367
47-2	1471	3.38	5.833
48-2	1598	3.38	5.923
49-2	1277	3.28	5.343
50-2	1591	3.49	5.891
51-2	1360	3.48	5.625
52-2	1564	3.60	5.911
53-2	1748	3.59	6.210
54-2	1748	3.64	6.154
55-2	1544	3.63	5.812
57-2	1303	3.28	5.441
58-2	1349	3.39	5.335
59-2	1375	3.43	5.557
60-2	1379	3.54	5.615
89-2	1880	3.57	6.413
Mole fraction NO_2 = 1.527 x 10^{-1}; Initial pressure = 0.03 atm			
152-2	1176	7.56 x 10^{-4}	5.402
151-2	1162	7.46 x 10^{-4}	5.382
150-2	1269	7.72 x 10^{-4}	5.462
149-2	1478	7.56 x 10^{-4}	5.649
148-2	1364	7.89 x 10^{-4}	5.498
147-2	1224	7.36 x 10^{-4}	5.417
146-2	1053	6.96 x 10^{-4}	5.220

E. References

1. M. Bodenstein and H. Ramstetter, Z. physik. Chem., 100, 106 (1922).

2. M. Bodenstein and F. Lindner, Z. physik. Chem., 100, 82 (1922).

3. L. S. Kassel, Kinetics of Homogenous Gas Phase Reactions, Chemical Catalog Company, New York (1932), p. 156.

4. D. R. Herschbach, H. S. Johnston, K. S. Pitzer and R. E. Powell, J. Chem. Phys., 25, 736 (1956).

5. W. A. Rosser, Jr. and H. Wise, ibid., 24, 493 (1956).

6. P. G. Ashmore and B. P. Levitt, Research (Correspondence), 9, 525 (1956).

7. G. Schott and N. Davidson, J. Am. Chem. Soc., to be published April, 1958.

8. N. Davidson and G. Schott, J. Chem. Phys., 27, 317 (1957); P. G. Ashmore and B. P. Levitt, ibid., 27, 318 (1957).

9. M. Steinburg and T. F. Lyon, abstract of paper presented before Inorganic and Physical Chemistry Section, 131st National Meeting, American Chemical Society, Miami, Florida, April, 1957.

10. T. Carrington and N. Davidson, J. Phys. Chem., 57, 418 (1953).

11. D. Britton, N. Davidson, W. Gehman, and G. Schott, J. Chem. Phys., 25, 804 (1956).

12. D. Britton, N. Davidson, and G. Schott, Discussions Faraday Soc. No. 17, 58 (1954).

13. F. W. Geiger and G. W. Mautz, The Shock Tube as an Instrument for the Investigation of Transonic and Supersonic Flow Patterns, Report on Contract N6-ONR-232, Project M720-4, Engineering Research Institute, University of Michigan (1949).

14. I. I. Glass, W. Martin, and G. M. Patterson, A Theoretical and Experimental Study of the Shock Tube, Report No. 2, Institute of Aerophysics, University of Toronto (1953).

15. T. C. Hall, Jr. and F. E. Blacet, J. Chem. Phys., 20, 1745 (1952).

16. G. Schott, Thesis, California Institute of Technology (1956).

17. D. Britton, Thesis, California Institute of Technology (1955)

18. D. M. Yost and H. Russell, Jr., Systematic Inorganic Chemistry, Prentice-Hall Inc., New York (1946), p. 28.

19. Handbook of Supersonic Aerodynamics, Navord Report 1488, Volume 2, Bureau of Ordnance, Department of the Navy (1950), pp. 502-502.113.

20. Selected Values of Chemical Thermodynamic Properties, National Bureau of Standards, Washington, D.C., Series III (1954).

21. H W. Wooley, The NBS-NACA Tables of Thermal Properties of Gases, National Bureau of Standards, Washington, D.C., Tables 15.10 and 15.11 (1950).

22. Selected Values of Chemical Thermodynamic Properties, National Bureau of Standards, Washington, D.C., Circular 500, Series I (1952).

23. H. W. Ford and N. Endow, J. Chem. Phys., 27, 1156 (1957).

24. A. A. Frost and R. G. Pearson, Kinetics and Mechanism, John Wiley and Sons, Inc., New York (1953), p. 71.

25. Ibid., pp. 67-70.

II. KINETICS OF THE FERROUS ION-OXYGEN REACTION IN SULFURIC ACID SOLUTION

This section consists of a paper published with

Professor Norman Davidson

in the Journal of the American Chemical Society

during 1956

[Reprinted from the Journal of the American Chemical Society, **78**, 4836 (1956).]

[CONTRIBUTION NO. 2099 FROM THE GATES AND CRELLIN LABORATORIES, CALIFORNIA INSTITUTE OF TECHNOLOGY]

Kinetics of the Ferrous Iron–Oxygen Reaction in Sulfuric Acid Solution

BY ROBERT E. HUFFMAN AND NORMAN DAVIDSON[1]

RECEIVED MAY 7, 1956

The reaction $4Fe^{II} + O_2 \rightarrow 4Fe^{III} + 2H_2O$, at 140–180° in 1 F H_2SO_4, proceeds by simultaneous bimolecular and termolecular reaction paths: $-d(Fe^{II})/dt = k_b(Fe^{II})P_{O_2} + k_t(Fe^{II})^2P_{O_2}$. At 159°, $k_b = 1.93 \times 10^{-5}$ atm.$^{-1}$ sec.$^{-1}$, $k_t = 1.60 \times 10^{-3}\ M^{-1}$ atm.$^{-1}$ sec.$^{-1}$; the respective activation energies were measured as 13.4 (±2) and 16.3 (±2) kcal. At 30.5°, only the termolecular path is observed (contrary to the predictions of the high temperature activation energies); $k_t = 2.78 \times 10^{-6}\ M^{-1}$ atm.$^{-1}$ sec.$^{-1}$ (1 F H_2SO_4). The variation of rate with $SO_4^=$ ($\mu \sim 1$, $NaClO_4$) indicates independent reactions, $2Fe^{++} + O_2 \xrightarrow{(1/2)k_u} 2Fe^{III} + H_2O_2$, and $FeSO_4 + Fe^{++} + O_2 \xrightarrow{(1/2)k_s} 2Fe^{III} + H_2O_2$, where $k_u = 1.4 \times 10^{-6}$ $k_s = 3.1 \times 10^{-5}\ M^{-1}$ atm.$^{-1}$ sec.$^{-1}$, and $K_{FeSO_4} = 1.1\ M^{-1}$. The reaction rate increases a small amount with increasing pH. Catalysis by Cu^{++} follows the rate law $-d(Fe^{++})/dt = 4k_9(Fe^{II})(Cu^{++})$ and is probably initiated by $Fe^{II} + Cu^{++} \xrightarrow{k_9} Fe^{III} + Cu^{I}$. In 0.23 F H_2SO_4, 0.35 F Na_2SO_4, $k_9 = 1.9 \times 10^{-3}\ M^{-1}$ sec.$^{-1}$. The rate-determining step for the bimolecular path is presumably either: (1a) $Fe^{II} + O_2 \rightarrow Fe^{III} + HO_2$, or (1b) $Fe^{II} + O_2 \rightarrow Fe^{IV} + H_2O_2$; for the termolecular path it is $2Fe^{II} + O_2 \rightarrow 2Fe^{III} + H_2O_2$. Possible detailed mechanisms are discussed. There is evidence that the bimolecular path, the termolecular path and the Cu^{++} catalyzed path are all accelerated by complexing anions, X, and to an extent depending on the affinity of X for Fe^{+++}. Furthermore, strong complexers favor the occurrence of the bimolecular path.

The rate of oxidation of ferrous ion by molecular oxygen in acid solution is very dependent upon the nature of the anions present. The rate increases as the complexing affinity of the anion for ferric ion increases. (It is to be expected that the complexing affinity for ferrous ion would be in the same order.) Thus, at a given pH, the rate is found to decrease in the series pyrophosphate,[2] phosphate,[3] chloride,[4,5] sulfate[6] and perchlorate.[7] The rate law is $-d(Fe^{II})/dt = 4k(Fe^{II})P_{O_2}$ for the first three media listed above and $-d(Fe^{II})/dt = 4k(Fe^{II})^2 \cdot P_{O_2}$ for the last two. The rate-determining steps are believed to be either (1a) or (1b) for the former case, and (2) for the latter.

$$Fe^{II} + O_2 \longrightarrow Fe^{III} + HO_2 \qquad (1a)$$

$$Fe^{II} + O_2 \longrightarrow Fe^{IV} + H_2O_2 \qquad (1b)$$

$$Fe^{II} + O_2 + Fe^{II} \longrightarrow 2Fe^{III} + H_2O_2 \qquad (2)$$

(1) We are indebted to the Atomic Energy Commission for support of this research under contract AT(11-1)-188, and to the General Education Board for a scholarship for one of us (R.H.). This paper was presented at the 129th National Meeting of the American Chemical Society, Dallas, Texas, April, 1956.

(2) J. King and N. Davidson, unpublished.

(3) M. Cher and N. Davidson, THIS JOURNAL, **77**, 793 (1955).

(4) J. W. McBain, *ibid.*, **5**, 623 (1901).

(5) A. M. Posner, *Trans. Faraday Soc.*, **49**, 382 (1953).

(6) A. B. Lamb and L. W. Elder, THIS JOURNAL, **53**, 137 (1931).

(7) P. George, *J. Chem. Soc.*, 4349 (1954).

Reaction (1a) is the first step in the Weiss one-electron oxidation mechanism.[8,9] The reactions as written are not balanced with respect to hydrogen ion; they are intended to indicate the oxidation changes involved but not to specify the dependence of rate upon acidity. The symbol (Fe^{II}) is defined as the formal concentration of ferrous iron; (Fe^{++}) means the concentration of the uncomplexed ion. A similar convention is used for other atomic species.

It was thought that the bimolecular reaction (1a or 1b), which involves one of the unstable intermediates, HO_2 or Fe^{IV}, would have a higher activation energy than the termolecular path (2) and would be more important at high temperatures. We have accordingly studied the ferrous iron, oxygen reaction at 140–180° in sulfuric acid. These results prompted a further investigation of the reaction in various solutions of sulfuric acid and sodium sulfate at room temperature and at ferrous iron concentrations considerably lower than those used by previous investigators. Some information on the cupric ion catalyzed reaction was also obtained.

Experimental

The experimental techniques for the high and low temperature reactions were different and will be described separately. The amount of ferric ion produced at given times was determined in both cases by measuring the ultraviolet absorption of the ferric sulfate complex ion[10] with a Beckman DU spectrophotometer.

Reagent grade ferrous ammonium sulfate, ferric ammonium sulfate, cupric sulfate and sodium sulfate were used. Sulfuric and perchloric acid solutions were prepared from concentrated reagent grade acids. Sodium perchlorate was prepared by neutralizing sodium hydroxide solutions with perchloric acid. The water used for high temperature reactions was prepared by redistilling tap distilled water from alkaline permanganate solution in a Pyrex, electrically heated still. The commercial redistilled water used in the first low temperature studies was found to contain trace amounts of copper. The water used in all results reported here at room temperature was prepared by redistilling the commercial distilled water in a Pyrex, electrically heated still to remove these traces of copper. In all cases, precautions were taken to exclude dust and to rinse vessels with the pure distilled water before preparing solutions. Tank oxygen was bubbled through water and filtered through glass wool before use.

A high temperature reaction cell consisted of an 8 cm. length of 15 mm. Pyrex tubing and, as a neck, an 11 cm. length of 5 mm. tubing. About 5 ml. of reaction solution was added, and air was displaced by a stream of O_2 gas introduced through a narrow capillary. The neck was then quickly sealed off in the middle while a stream of O_2 was still passing through the top of the neck.

The sealed reaction tubes were wrapped in glass wool and placed in short sections of iron pipe closed with pipe caps. The high temperatures were provided by a silicone oil-bath, and temperature control was by means of a mercury thermoregulator. The iron pipes containing the reaction cells were attached to a chain and sprocket wheel arrangement which rotated the iron pipes end over end in the bath, thus stirring the reaction tubes and the bath. The bath was allowed to heat up about 15° above the controlled temperature just before placing the stirrer and iron pipes therein. This reduced the time necessary to bring the reaction cells up to the high temperature. At the end of a reaction period, usually two hours, the reaction was quenched by cooling the pipes rapidly in cold water. The reaction tubes were placed in a one cm. Beckman cell holder drilled out to hold the cylindrical tubes. The absorption spectrum of the iron (III)–sulfate system is dependent upon temperature. Optical density measurements between 340 and 410 mμ were made using a cell compartment thermostated at 33°. As compared to flat faced cells, the blank optical densities of the tubular reaction cells containing either 1 *F* sulfuric acid or water were about 0.180 to 0.080, depending on the wave length. Rough values for the effective extinction coefficient, ϵl in the expression $D = c\epsilon l$ are 1300, 200 and 36 at wave lengths of 340, 375 and 400 mμ, respectively. The reaction cells were calibrated after each reaction by measuring the absorption spectra of ferric ammonium sulfate solutions in the same sulfuric acid medium. We are indebted to Mr. John Andelin who constructed the high temperature bath and made a few preliminary runs.

The room temperature reactions, which were very slow, were carried out in Pyrex absorption cells, 5 cm. in diameter by 10 cm. long, with Corex windows. It was possible to make measurements at 310 mμ, where the complex has its maximum absorption. The cells had a total volume of 150–175 ml., and about 100 ml. of solution was used. Oxygen was added and the cells sealed as described above. The absorption cells were rotated slowly in a water-bath at 30.5°. At intervals of several hours, they were removed for optical density measurements and then replaced in the bath.

In both temperature ranges, the pressure or partial pressure of oxygen was essentially constant because there was a sufficiently large gas space above the solution.

Special care was taken to remove dust particles and traces of iron salts from the reaction vessels. The inside of the vessel was washed with hot aqua regia or nitric acid, thoroughly rinsed with distilled water, dried in an oven, and then protected from dust until the reaction solution was placed in it.

Results

Effects of Fe^{II} and Fe^{III} Concentrations. (a) **High Temperatures.**—In the range 140–180°, at ferrous ion formal concentrations between 0.00100 and 0.0250 *F*, the oxygenation was found to proceed by two independent reaction paths—one first order in ferrous ion and in oxygen, and one second order in ferrous ion and first order in oxygen—that is, according to the rate law

$$-\frac{\mathrm{d}\ln(Fe^{II})}{\mathrm{d}t} = k_b P_{O_2} + k_t(Fe^{II})P_{O_2} \qquad (3)$$

where k_b and k_t may be functions of the sulfate and hydrogen ion concentrations as well. This rate law accounts for the change in rate during the course of a reaction and for the variation of initial rate with initial concentration. Added Fe^{III} does not affect the rate.

Since the oxygen pressure remains constant during a reaction, it would be expected that plots of $\log (Fe^{II})_i/(Fe^{II})_t$ *vs.* t would be linear for a first-order dependence on ferrous ion. $(Fe^{II})_i$ and $(Fe^{II})_t$ are the ferrous ion concentrations initially and at time t. Figure 1 shows that these plots are concave downward. However, plots of $1/(Fe^{II})$ *vs.* t are concave upward.

The constants k_b and k_t were evaluated as follows. An apparent first-order rate constant, k', is defined by

$$k' = \frac{-\ln(Fe^{II})_{t_2}/(Fe^{II})_{t_1}}{t_2 - t_1}$$

for various times of reaction, where the interval between t_2 and t_1 is 1 hr. According to (3)

$$k' = k_b P_{O_2} + k_t(Fe^{II})P_{O_2}$$

The quantity k' is taken to apply to the average of $(Fe^{II})_{t_2}$ and $(Fe^{II})_{t_1}$; plots of k' *vs.* (Fe^{II}) were linear, as expected from (3), and were extrapolated to the initial ferrous ion concentration to give k'_i,

(8) J. Weiss, *J. Chim. Phys.*, **48**, C-6 (1951).

(9) J. Weiss, *Experientia*, **IX**, 61 (1953).

(10) R. W. Whiteker and N. Davidson, THIS JOURNAL, **75**, 3081 (1953).

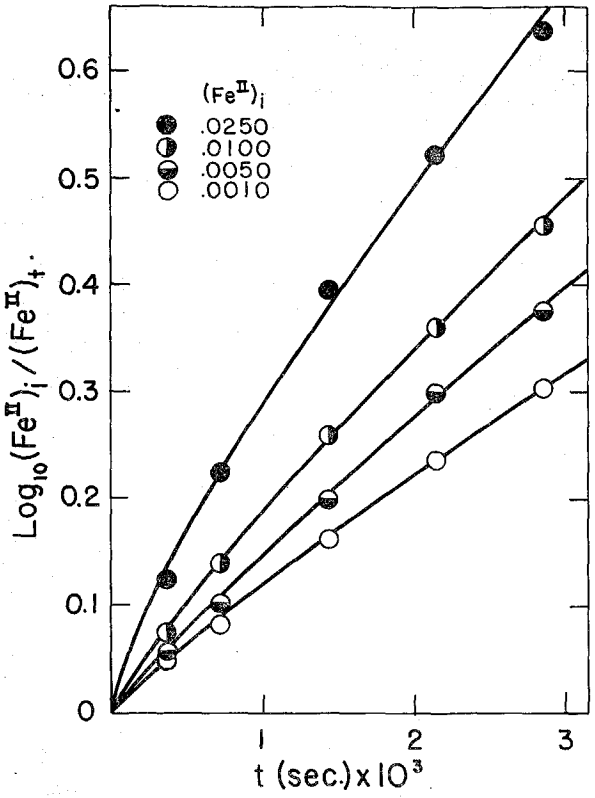

Fig. 1.—First-order plots for typical high temperature reactions (159°, 1.00 *F* H_2SO_4, in oxygen).

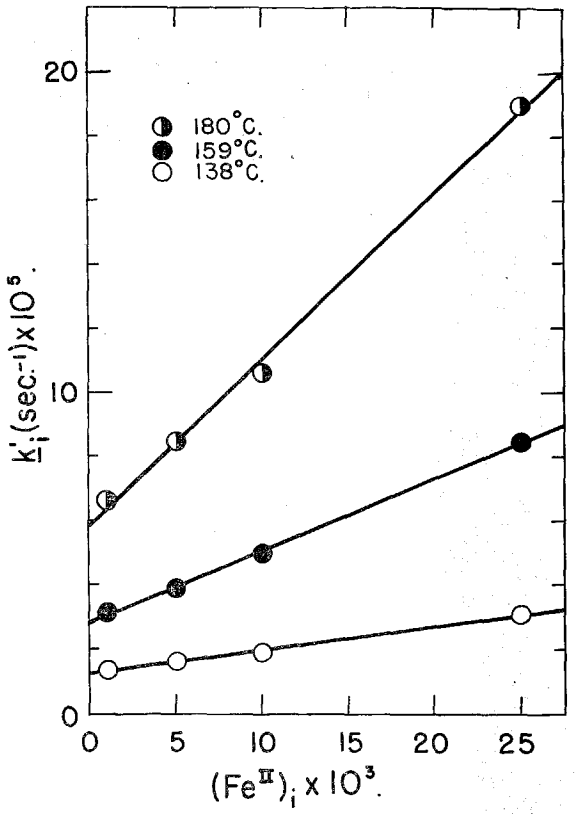

Fig. 2.—Variation of initial d ln $(Fe^{II})/dt$ with $(Fe^{II})_i$.

the initial apparent first-order constant. Values of k'_i at the same initial ferrous ion concentrations and temperatures were averaged and the averages plotted against the initial ferrous ion concentration. The straight lines obtained confirm equation 3 and are exhibited in Fig. 2. The resulting values of k_b and k_t are given in Table I. Activation energies of 13.4 (± 2) and 16.3 (+ 2) kcal. were obtained for the second-order and third-order paths, respectively, from plots of log *k vs.* $1/T$. The points fit on the appropriate straight lines to ±15% giving rise to the indicated uncertainties.

TABLE I

HIGH TEMPERATURE RATE AND CONSTANTS

Initial Fe^{II} (mole $l.^{-1}$)	0.00100	0.00200	0.00500	0.0100	0.0250		
T, °C.			k_i' (sec.$^{-1}$) × 10^5			k_b[a] (sec.$^{-1}$ atm.$^{-1}$) × 10^5	k_t[a] (sec.$^{-1}$ atm.$^{-1}$ M^{-1}) × 10^3
138	1.38		1.65	1.86	3.14	0.89	0.55
159	3.11		3.88	5.00	8.50	1.93	1.60
161	3.02	3.16	3.52	4.72		1.90	1.33
180	6.65		8.44	10.6	19.0	3.84	3.40

[a] P_{O_2} calculated from initial pressure of one atmosphere at room temperature assuming perfect gas law.

Inhibition of the reaction by ferric ion was not found. At 160° in 1.00 *F* H_2SO_4 with an oxygen atmosphere, the reaction in solutions initially 0.00500 *F* in ferrous ion and 0.00100, 0.00500, 0.0100 and 0.0200 *F* in ferric ion were unaffected by the added ferric ion within the experimental error of 5%. Solutions initially 0.00100 and 0.00200 *F* in ferrous ion containing 0.0100 *F* ferric ion initially gave no indication of ferric ion inhibition.

(b) Room Temperature.—The values for k_b and k_t at 30° predicted by extrapolation of the high temperature measurements are 2.5×10^{-8} sec.$^{-1}$ atm.$^{-1}$ and 3.5×10^{-7} sec.$^{-1}$ M^{-1} atm.$^{-1}$ (M = mole liter^{-1}). This suggested that the second-order path would make a contribution to the rate equal to that of the third-order path for (Fe^{II}) = 0.07 *M*. Previous investigators have worked at concentrations of 0.15–0.20 *M*,[6] 0.02–0.46 *M*,[4] and 0.01–0.3 *M*.[7] For the present investigations, measurements were obtained for only a few per cent. reaction, and the initial rate was determined from a plot of (Fe^{III}) *vs. t*. The initial rates were plotted as $-\text{d ln}(Fe^{II})/dt$ *vs.* $(Fe^{II})_i$; the intercepts, which should have been $k_bP_{O_2}$, were smaller than the experimental error and oxygen independent. In 1.00 *F* H_2SO_4, $k_t = 2.78 \times 10^{-6}$ sec.$^{-1}$ M^{-1} atm.$^{-1}$ and $k_b = 3 \times 10^{-10}$ sec.$^{-1}$ atm.$^{-1}$ from rates obtained at four ferrous ion concentrations. The small contribution from the path first order in ferrous ion could be due partially to the first-order ferrous path found at high temperatures. The erratic behavior, however, indicates that this contribution is a combination of experimental error and small amounts of impurities. Values of k_t at 30.5° in two sulfuric acid–sodium sulfate solutions in air and oxygen are given in Table II.

Effect of Glass Surface.—Studies with added Pyrex glass wool showed that catalysis by the walls of the reaction cells was probably not important. The first experiments at 140–180° gave erratic results, with some reactions proceeding very

TABLE II

RATE DATA AT 30.5°

$(Fe^{II})_i$, F	$-d(Fe^{II})/dt$ (M sec.$^{-1}$)		Ratio of rates (oxygen/air)
	1.00 F H_2SO_4		
	air ($\times 10^{12}$)	oxygen ($\times 10^{12}$)	
0.00100	6.62	6.55	
.00500	17.8	66.1	
.0100	55.0	284	
.0200	224	1130	
[a]			
l_t (sec.$^{-1}$ M^{-1})	5.47×10^{-7}	2.78×10^{-6}	5.1
l_b (sec.$^{-1}$)	3.9×10^{-10}	~0	0
	0.226 F H_2SO_4 and 0.354 F Na_2SO_4		
$(Fe^{II})_i$, F	air ($\times 10^{12}$)	oxygen ($\times 10^{12}$)	
0.00100	4.86	8.68	
.00500	44.5	143	
.0100	139	540	
.0200	545	2320	
l_t (sec.$^{-1}$ M^{-1})	1.18×10^{-6}	5.65×10^{-6}	4.8
l_b (sec.$^{-1}$)	3.1×10^{-9}	1.7×10^{-9}	0.5

[a] $-d(Fe^{++})/dt = l_b(Fe^{II}) + l_t(Fe^{II})^2$.

rapidly. Fairly reproducible results were obtained when the glass wool was heated to 500° in an oven for one-half hour, washed in hot aqua regia, rinsed, dried and transferred to the reaction cell with a glass rod. The glass wool could be centrifuged to the bottom of the cell for optical measurements.

The surface area[3] of the glass wool is estimated as 2300 cm.^{2} g.$^{-1}$. The additional surface area due to the glass wool was around three times the total inside wall area of a reaction cell. With $(Fe^{II})_i$ = 0.001 to 0.005 M, in oxygen, the ratio of reaction rates in the presence and absence of glass wool varied in an erratic fashion between 1.3 and 1. Thus it appears that the wall reaction was probably never more than 10% of the homogeneous reaction in the unpacked cells. Reaction rates in unpacked cells were more reproducible than in packed cells, suggesting that the cleaning procedure was effective and reproducible for the glass walls of the cells.

Experiments at 30.5° with added glass wool were carried out in glass stoppered bottles and the solutions siphoned back and forth between optical cells with an all-glass siphon system. With $(Fe^{II})_i$ between 0.001 and 0.02 M, there was less than 1% effect that could be attributed to the walls of the optical cells.

Effect of Oxygen Pressure.—The first results obtained at 30.5° for the ratio of reaction rates in oxygen and in air at 1 atm. pressure were not the expected 4.76:1. A long and tedious set of measurements indicated that there was a reaction path that was first order in ferrous ion and zero order in oxygen and a reaction path that was second order in ferrous ion and first order in oxygen. A great deal of time was wasted before it was discovered that the commercial distilled water being used contained traces of cupric ion, which was responsible for the oxygen independent path.

At a fixed oxygen partial pressure, we may define apparent first- and second-order rate constants, referring to the dependence of rate on (Fe^{II}); $-d(Fe^{II})/dt = l_b(Fe^{II}) + l_t(Fe^{II})^2$. In redistilled water, containing no significant Cu^{II}, the ratio of l_t in oxygen and air was evaluated as 5.1 in 1.00 F H_2SO_4 and 4.8 in a solution 0.226 F in H_2SO_4 and 0.354 F in Na_2SO_4, whereas the quantity l_b was very small and evidently inversely dependent on oxygen pressure (Table II). It seems probable that the apparent first-order path is a residual effect due to impurities and experimental error; the main part of the reaction proceeds by the rate law, $-d(Fe^{II})/dt = l_t(Fe^{II})^2 = k_t(Fe^{II})^2 P_{O_2}$.

The oxygen dependence was investigated at 160° in 1.00 F H_2SO_4, where reaction paths first and second order in ferrous ion had been found to occur. One run at each of two initial ferrous ion concentrations in air and oxygen was made. The ratio of the l_t values for the path second order in ferrous ion was 5.4 and the ratio of the l_b values for the path first order in ferrous ion was 3.5. The value of 3.5 is not entirely satisfactory. These reactions at high temperatures were carried out using the same 1.00 F H_2SO_4 that was used at low temperatures, and it is known definitely that cupric ion is in very low concentration ($\sim 1 \times 10^{-7}$ F). The reaction between cupric ion and ferrous ion, which is a reasonable first step for cupric ion catalysis, would probably not be favored by an increase in temperature. The fact that the ratio of rate in oxygen to rate in air is not erratic and is 3.5 indicates that some of the path first order in ferrous ion must be oxygen dependent. We believe that the data indicate that the main part of the term in the rate law that is first order in (Fe^{II}) is also first order in oxygen. The discrepancy between 3.5 and the expected 4.8 may be partially due to impurities. It may also be partially due to errors in determining both l_b and l_t from the data on change in initial rate with $(Fe^{II})_i$ at any one oxygen pressure. The fact that the ratio, 5.4, of l_t in oxygen and air is higher than expected is consistent with this possibility.

Effect of Sulfate and Hydrogen Ion.—The effects of varying the sulfate ion at approximately constant hydrogen ion concentration and varying the hydrogen ion at relatively constant sulfate ion concentrations have been studied at 30.5° in one atmosphere of oxygen in solutions 0.0200 and 0.0400 F in ferrous ion. Stock solutions were prepared by dissolving various amounts of sodium sulfate and sulfuric acid in water that had been redistilled to remove traces of cupric ion. The solutions were kept at an ionic strength of 1.0–1.3 with sodium perchlorate. These results are uncertain in that a value for the second ionization constant for sulfuric acid must be chosen. We have taken this value to be 0.075 at an ionic strength of 1.0 (sodium perchlorate).[10] The dependence of the third-order rate constant k_t on sulfate ion is seen in Fig. 3. The hydrogen ion was varied from 0.066 to 0.099 M in this series but, as will be seen later, this will have little effect. The rate constant increases at a decreasing rate as the sulfate ion concentration is increased. The increase in the sulfate ion concentration and the slight increase in optical density of the reaction solution due to the large

amounts of ferrous ammonium sulfate added have been taken into account.

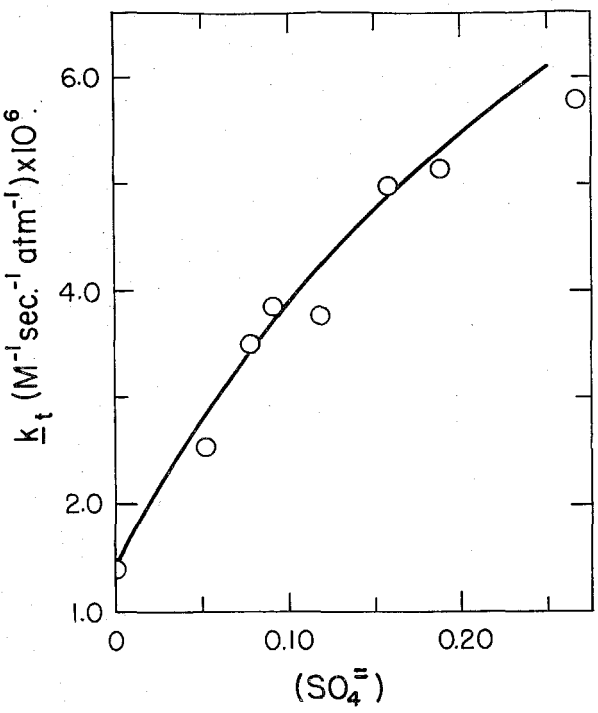

Fig. 3.—Dependence of termolecular rate constant at 30.5° on sulfate ion concentration. Reactions in oxygen at one atmosphere pressure. The formal concentrations of the various added chemicals, and the calculated concentrations of some of the ions (assuming $K_{HSO_4^-} = 0.075$) are displayed below. μ = 1.0–1.3 (sodium perchlorate).

(H_2SO_4), F	(Na_2SO_4), F	(Fe^{II}), F	($SO_4^=$), M	(H^+), M	(HSO_4^-), M
0.068	0	0.020	0.052	0.080	0.056
		.040	.078	.066	.070
.094	.061	.020	.091	.084	.104
		.040	.118	.071	.117
.135	.166	.020	.158	.087	.183
		.040	.118	.077	.193
.226	.354	.020	.267	.099	.353

The increase in the rate constant can be explained by the following argument. At zero sulfate ion concentration, the path second order in ferrous ion should be the same as the path in perchloric acid, where little complexing is to be expected. From data of George,[7] the constant for this reaction is found to be 1.4×10^{-6} M^{-1} atm.$^{-1}$ sec.$^{-1}$ in 0.083 F $HClO_4$ at 30° and an ionic strength of 1.0. When this value is placed on Fig. 3, it is possible to draw a smooth curve through the points. A reasonable mechanism for sulfate ion catalysis would seem to be

$$2Fe^{++} + O_2 \xrightarrow{k_u} 2Fe^{III} + H_2O_2 \qquad (4)$$

as an uncatalyzed rate step, and

$$Fe^{++} + SO_4^= \underset{}{\overset{K}{\rightleftharpoons}} Fe^{++}SO_4^= \qquad (5)$$

$$Fe^{++}SO_4^= + Fe^{++} + O_2 \xrightarrow{k_s} 2Fe^{III} + H_2O_2 + SO_4^= \qquad (6)$$

for the sulfate-catalyzed rate step. This mechanism would lead to the rate expression

$$\frac{-d(Fe^{II})}{dt} = k_u(Fe^{++})^2P_{O_2} + k_s(FeSO_4)(Fe^{++})P_{O_2} = k_t(Fe^{II})^2P_{O_2} \qquad (7)$$

If all ferrous ion is either uncomplexed or as the ferrous-sulfate complex, the following expressions may be obtained, where (Fe^{II}) is the formal ferrous ion concentration.

$$\frac{(FeSO_4)}{(Fe^{II})} = \frac{K(SO_4^=)}{1 + K(SO_4^=)} \qquad \frac{(Fe^{++})}{(Fe^{II})} = \frac{1}{1 + K(SO_4^=)}$$

Substituting these expressions into (7), one obtains

$$k_t = \frac{k_u + k_sK(SO_4^=)}{1 + K(SO_4^=)^2} \qquad (8)$$

By setting $k_u = 1.4 \times 10^{-6}$ M^{-1} atm.$^{-1}$ sec.$^{-1}$ as found by George, and assuming the sulfate ion concentration is not appreciably affected by the ferrous sulfate complex, expression (8) may be solved numerically for k_s and K by using values of k_t and ($SO_4^=$) from Fig. 3. Values obtained were $K = 1.1 \pm 0.2$ M^{-1} and $k_3 = 3.1 \pm 0.5 \times 10^{-6}$ M^{-1} atm.$^{-1}$ sec.$^{-1}$. The curve shown in Fig. 3 is the theoretical curve drawn from (8) with these values.

The results obtained by varying the hydrogen ion concentration are shown in Table III. The hydrogen ion dependence of the reaction is uncertain from these experiments in that the sulfate ion concentration has not been controlled as well as desired. This makes detailed kinetic interpretation difficult. However, as the hydrogen ion concentration is decreased by a factor of 75 from 1.032 to 0.014, the rate constant at most doubles. Also, the rate constant does not change drastically over the hydrogen ion concentrations which were obtained in the sulfate dependence experiments. We have no satisfactory explanation for the observed small dependence upon hydrogen ion concentration. A generally similar dependence of the termolecular rate constant on H^+ is observed in perchlorate media.[7]

TABLE III

HYDROGEN ION DEPENDENCE

H_2SO_4, F	Na_2SO_4, F	Fe(II), F	($SO_4^=$), M	(H^+), M	(HSO_4^-), M	k_t (M^{-1} sec.$^{-1}$ atm.$^{-1}$) x 10^6
1.00	0.0	0.0200	0.072	1.032	0.968	2.78
0.466	.040	.0200	.075	0.461	.471	3.17
		.0400	.086	.432	.500	3.00
.094	.061	.0200	.091	.084	.104	3.86
		.0400	.118	.071	.117	3.78
.0203	.0664	.0200	.104	.017	.023	5.28
		.0400	.141	.014	.026	5.05

All rate determinations in this investigation were made on solutions of ferrous ammonium sulfate. By adding an equal concentration of ammonium sulfate to a typical high temperature reaction in 1.00 F H_2SO_4 under oxygen, the ammonium ion was shown to be without effect on the reaction rate.

Possible Effects of Organic Impurities.—In the high temperature range, it was thought that residual organic dust impurities might participate in induced reactions, or otherwise enter into the

reaction and be destroyed in the process. To check on this possibility, solutions with $(Fe^{II})_i$ = 0.001 to 0.005 *F* in 1.00 *F* sulfuric acid were heated at 160° in oxygen to about 60% reaction. The tubes were then carefully opened, and a small, known volume of a concentrated ferrous ion solution was added. The tubes were then resealed in oxygen and reheated. The observed rate constants were the same before and after addition of the concentrated ferrous ion solution. Since there was no decrease in rate constant after addition of the concentrated ferrous ion solution, either reaction with organic dust impurities is not occurring, or the concentration of these impurities is too large to be appreciably reduced by the reaction.

Effect of Cu(II).—As described previously, the anomalous results first obtained at 30.5° led us to suspect Cu^{II} as an impurity. Trace analyses for Cu^{II} were therefore made using a spectrophotometric method based on the dithizone–cupric ion complex.[11] Sulfuric acid, sodium sulfate, ferrous ammonium sulfate and sodium perchlorate solutions were found not to contain significant concentrations of cupric ion. However, commercial distilled water contained concentrations of *ca.* 2×10^{-6} *F* Cu^{II}. In redistilled water, the cupric ion concentration was reduced at least twenty times to a value which would not significantly affect the rate.

At 30.5° in sulfuric acid–sodium sulfate solutions, cupric ion catalyzes the ferrous ion–oxygen reaction by a reaction path first order in ferrous ion, first order in cupric ion and zero order in oxygen pressure. These results have been obtained in a stock solution 0.226 *F* in H_2SO_4 and 0.354 *F* in Na_2SO_4, which has (H^+) = 0.11 *M*, (HSO_4^-) = 0.34 and $(SO_4^=)$ = 0.24.

In these solutions, increasing the cupric ion concentration increases the rate of the reaction path first order in ferrous ion. It was found that the measured rate is a linear function of the total cupric ion concentration for reactions with $(Fe^{II})_i$ = 0.00100 *F* in air at one atmosphere. In reactions containing the relatively high total cupric ion concentration of 1.1×10^{-5} *F*, the rate is the same in air and oxygen. The rate law for this situation at given sulfate and hydrogen ion concentrations is

$$-d(Fe^{II})/dt = k_t(Fe^{II})^2P_{O_2} + 4k_9(Fe^{II})(Cu^{II})$$

The above equation with $k_9 = 1.9 \times 10^{-3}$ M^{-1} sec.$^{-1}$ and $k_t = 1.5 \times 10^{-5}$ M^{-1} atm.$^{-1}$ sec.$^{-1}$ fits the data to ±5%.

Since the concentrations of cupric and ferric ions are relatively low, the catalysis may be explained by the following reactions postulated by Cher and Davidson[3] and many previous workers.

$$Cu^{II} + Fe^{II} \xrightarrow{k_9} Cu^{I} + Fe^{III} \quad (9)$$

$$Cu^{I} + O_2 \longrightarrow Cu^{II} + HO_2 \quad (10)$$

It is assumed that the first reaction is the rate step and the second reaction is very rapid. The HO_2 reacts further with Fe^{II} as in the Weiss mechanism.[8]

(11) E. B. Sandell, "Colorimetric Determination of Traces of Metals," 2nd Ed., Interscience Publishers, Inc., New York, N. Y., 1950, p. 295.

Discussion

The activation energy for the bimolecular reaction measured between 140 and 180° is 13.4 (± 2) kcal. However, the upper limit for k_b at 30.5° combined with the average value, $k_b = 1.9 \times 10^{-5}$ sec.$^{-1}$ atm.$^{-1}$ at 160°, implies that $E_a > 22$ kcal. The activation energy for the termolecular reaction observed at high temperatures is 16.3 (± 2) kcal. The values at 160 and 30° imply E_a = 12.6 kcal. George[7] reports E_A = 17.4 kcal, for the termolecular path between 20 and 40° in 0.50 *F* $HClO_4$. The possibility of unknown experimental errors cannot, of course, be excluded. However, it would not be surprising if the activation energy for either reaction path were dependent on temperature. This is especially likely because there is probably a very marked change in the concentrations and activity coefficients of the ionic species present in 1*F* H_2SO_4 between 30° and the range 140–180°.

The experimental results do not, of course, distinguish between the alternative intermediate HO_2 and Fe^{IV} (reactions 1a and b) for the bimolecular reaction path. The Weiss mechanism[8] involves the former intermediate. In this case, the complete reaction path is

$$Fe^{II} + O_2 \longrightarrow Fe^{III} + HO_2 \quad (1a)$$

$$Fe^{II} + HO_2 \longrightarrow Fe^{III} + H_2O_2 \quad (11)$$

$$Fe^{II} + H_2O_2 \longrightarrow Fe^{III} + OH + OH^- \quad (12)$$

$$Fe^{II} + OH \longrightarrow Fe^{III} + H_2O \quad (13)$$

The observed values of k_b are four times the rate constant for reaction (1a) for this mechanism.

Experiments in this Laboratory have shown that in a pyrophosphate medium, the rate of oxygenation is first order in Fe^{II} and first order in oxygen,[2] and faster than the corresponding reaction rate in a phosphate medium. Weiss[9] has reported that the reaction is bimolecular with respect to Fe^{II} and O_2 in the presence of fluoride. Posner[5] reports a bimolecular reaction in 5–8 *F* HCl at room temperature, and the reaction rate decreased markedly with acidity. As discussed below, the data of McBain[4] indicate that the reaction is principally termolecular in 1 *F* HCl. In a perchlorate medium,[7] the reaction path at room temperature is exclusively termolecular, and no investigations have been made at high temperature.

Weiss[9] has proposed essentially the following as a model of the transition state

$$[X\text{---}Fe^{II}\text{---}O_2] \longleftrightarrow [X\text{---}Fe^{III}\text{---}O_2^-]$$

The transition state is stabilized by groups, X, which form complexes with tripositive iron. The equilibrium constants for the reaction

$$Fe^{+++} + X^{-n} \rightleftharpoons FeX^{3-n}$$

for $H_2P_2O_7^=$,[12] F^-,[13] $H_2PO_4^-$,[14] $SO_4^=$,[10] Cl^-,[15] ClO_4^-,[16] in the neighborhood of 25° are: 10^5, 5×10^5, 1.4×10^3, 100, 4.1, 1–3 mole^{-1} liter, respec-

(12) Preliminary estimate based on work in this Laboratory.

(13) H. W. Dodgen and G. K. Rollefson, THIS JOURNAL, **71**, 2600 (1949).

(14) T. Yamane and N. Davidson, to be published.

(15) M. W. Lister and D. E. Rivington, *Can. J. Chem.*, **33**, 1603 (1955).

(16) K. W. Sykes, *Chem. Soc. Special Pub. No. 1*, 64 (1954).

tively. Thus, in the presence of the strong complexes, the oxygenation is bimolecular at room temperature. For the complexing agents of moderate strength, $SO_4^=$ and Cl^-, the reaction is termolecular at room temperature and moderate (< 1 F) concentration of the complexing anions. A bimolecular reaction occurs in more extreme conditions—at high temperatures in 1 F H_2SO_4 or in 5 F HCl at room temperature. At room temperature in perchlorate media, the oxygenation is termolecular; it is not known whether a bimolecular reaction will occur for more extreme conditions. Suitable data for a quantitative comparison are not available, but the relative reaction rates for the bimolecular path generally parallel the complexing constants quoted above.

The rate-determining step for the termolecular path is probably

$$2Fe^{II} + O_2 \longrightarrow 2Fe^{III} + H_2O_2 \qquad (2)$$

followed by reactions (7) and (8). The observed values of k_t are therefore twice the rate constant of the above reaction. Two possible detailed models for reaction (2) are

$$(H_2O_2)_5Fe^{II}OH_2^{++} + O{=}O + H_2OFe^{II}(OH_2)_5^{++} \longrightarrow$$
$$(H_2O_2)_5Fe^{III}OH^{++} + H_2O_2 + HOFe^{III}(OH_2)_5^{++} \qquad (2')$$

$$(H_2O)_6Fe^{++} + O{=}O + Fe(H_2O)_6 \rightleftharpoons$$
$$(H_2O)_5Fe^{II}\ldots O{=}O\ldots Fe^{II}(H_2O)_5^{++++} \longrightarrow$$
$$(H_2O)_5Fe^{III}\text{–}O\text{–}O\text{–}Fe^{III}(H_2O)_5^{++++} \longrightarrow \qquad 2(")$$
$$(H_2O)_6Fe^{+++} + H_2O_2 + Fe(H_2O)_6^{+++}$$

Mechanism (2′) involves a hydrogen atom transfer from the water molecules of the coördination sphere of Fe^{++}. In mechanism (2″), an O_2 molecule is directly coördinated to two Fe^{++} ions, and a peroxide bridge between two Fe^{+++} ions is formed. It may be recalled that a peroxy complex of Fe^{III}, $Fe(O_2H)^{++}$, is known.[17,18] If (2′) were correct, there should be a marked hydrogen isotope effect and a significant decrease in reaction rate in D_2O, whereas this should not be the case for (2″). Evidence of this nature in favor of a hydrogen atom transfer mechanism for the Fe^{++}, Fe^{+++} electron exchange has recently been reported.[19] Evidence that there is no significant hydrogen isotope effect in the similiar Pu^{III}–Pu^{IV} oxygenation has been found recently.[18] In either case, it is plausible that sulfate ion would accelerate the rate because of complex ion formation in the transition state. Thus for case (2″), the transition state would be

$$(H_2O)_4(SO_4)Fe\text{–}O\text{–}O\text{–}Fe(H_2O)_5^{+4}$$

No independent evidence is available to compare with the deduction from the kinetic data that the complex constant of Fe^{++} with $SO_4^=$ is 1.1 mole^{-1} liter. The value is about as expected for these ions for an ionic strength of 1.0, however.

The termolecular rate constant k_t at 30.5° in 1 F H_2SO_4 found in this study, 2.78×10^{-6} M^{-1} atm.$^{-1}$ sec.$^{-1}$, agrees well with values reported by other investigators. Lamb and Elder[6] found 4.0×10^{-6} and McBain[4] reported 1.1×10^{-6}, in both cases at 30° in 1 F H_2SO_4. (The corresponding comparison made by George[7] between rates in $HClO_4$ and in H_2SO_4 is slightly erroneous in that Lamb and Elder's results were not corrected from 1 atm. air to 1 atm. O_2.) We find that the data of McBain in 1 F HCl fit a termolecular rate law much better than a bimolecular rate law; the rate constant (apparently at 30°) is 6.5×10^{-6} M^{-1} atm.$^{-1}$ sec.$^{-1}$.

The rate constant for the first step in the cupric ion catalyzed reaction is 1.9×10^{-3} M^{-1} sec.$^{-1}$

$$Fe^{II} + Cu^{II} \longrightarrow Fe^{III} + Cu^{I} \qquad (9)$$

in 0.226 F H_2SO_4, 0.354 F Na_2SO_4. The corresponding value in 0.434 F H_3PO_4, 0.302 F $H_2PO_4^-$ is 2.8×10^{-1}. This shows that phosphate ion complexes the iron in the transition state for reaction (9). Since sulfate is a moderately strong complexing anion for Fe^{+++}, it may be assumed that $SO_4^=$ can also participate in the transition state for reaction (9). Unfortunately, no data to test this prediction were obtained.

George[7] reports that the Fe^{II}, O_2 reaction in perchloric acid is only slightly catalyzed by Cu^{II}, and that the catalyzed reaction is second order in Fe^{II}. The smallness of the catalytic effect may in part be due to the slowness of reaction (9) in $HClO_4$. There is however an additional consideration. Cher and Davidson[3] observed that at high Cu^{II} concentrations, the mechanism of the Fe^{II}, O_2 reaction was

$$Fe^{II} + Cu^{II} \overset{K_9}{\rightleftharpoons} Fe^{III} + Cu^{I} \qquad (9)$$

$$Cu^{I} + O_2 \overset{K_{10}}{\rightleftharpoons} Cu^{II} + HO_2 \qquad (10)$$

$$Fe^{II} + HO_2 \overset{k_{11}}{\longrightarrow} Fe^{III} + H_2O_2 \qquad (11)$$

The corresponding rate expression is $-d(Fe^{II})/dt = 4\,k_{11}K_9K_{10}\,(Fe^{II})^2P_{O_2}/(Fe^{III})$, and the rate is independent of Cu^{II} concentration. K_9K_{10} is actually the equilibrium constant for the reaction

$$Fe^{II} + O_2 \rightleftharpoons Fe^{III} + HO_2 \qquad (12)$$

The value of this equilibrium quotient in 1 F $HClO_4$ may be estimated as 3×10^{-4} of its value in 0.43 F H_3PO_4, 0.30 F $H_2PO_4^-$ from the formation constants of $Fe(H_2PO_4)^{++}$ and $Fe(H_2PO_4)_2^+$ (1.4×10^3 mole^{-1} liter and 3.4×10^4 mole^{-2} liter^2).[14] Reaction (10) is a fast, exothermic reaction and possibly not greatly affected by complexing anions. On this basis, we estimate from the results of Cher and Davidson[3] that the rate law for the copper catalyzed reaction in 1 F $HClO_4$ is $-d(Fe^{II})dt = 8 \times 10^{-7}\,(Fe^{II})^2P_{O2}/(Fe^{III})$; the rate law for the uncatalyzed reaction is $2 \times 10^{-6}(Fe^{II})^2P_{O_2}$. It is not expected that the above calculation is very reliable, but it does suggest that after the accumulation of some Fe^{III} in the system, the copper catalyzed reaction might indeed be rather insignificant in comparison to the uncatalyzed *termolecular* reaction.

PASADENA, CALIFORNIA

(17) M. G. Evans, D. George and N. Uri, *Trans. Faraday Soc.*, **45**, 230 (1949).

(18) We are indebted to Dr. T. W. Newton for some interesting corespondence regarding the possibility of (2″).

(19) J. Hudis and R. W. Dodson, THIS JOURNAL, **78**, 911 (1956).

III. PROPOSITIONS

1. Study of the high temperature decomposition of NO to N_2 and O_2 between 2000 and 3000°K has indicated a mechanism involving O and N atoms, as proposed by Zeldovitch from experiments on explosions in air (1). The data of Glick, Klein, and Squire (2), who studied air reactions with a single pulse shock tube technique, support the mechanism. However, Fenimore and Jones (3), who studied NO decomposition in a flame, did not observe the predicted inhibition term $k_3[NO]/k_2[O]$ even though [NO]/[O] was varied from .5 to 2000. There are several indications that k_3 and k_4 are comparable. It is proposed to study the decomposition of NO with the single pulse shock tube technique to resolve this question.

(1) J. Zeldovitch, Acta Physico. URSS 21, 577 (1946).

(2) H. S. Glick, J. J. Klein, and W. Squire, J. Chem. Phys. 27 850 (1957).

(3) C. P. Fenimore and G. W. Jones, J. Phys. Chem. 61, 654 (1957).

2. The reaction between ferric ion and iodide ion has been assumed to involve a ferric ion-iodide ion complex as the initial reaction step (3). A spectrophotometric method involving a fast mixing apparatus is proposed to detect and study this complex.

(3) A. J. Fudge and K. W. Sykes, J. Chem. Soc. 1952 119.

3. It has been postulated that in the urea-formaldehyde reactions leading to polymer formation urea acts as an amino acid amide (4). Results of more recent analyses and kinetics studies do not support such an interpretation (5). It is proposed that several of the arguments supporting the amino acid amide theory are unconvincing, and other experiments are proposed to test the theory. Two such experiments are the reaction of ethylene diamine and oxamide with formaldehyde.

(4) C. S. Marvel, J. R Elliot, F. E. Boettner, and H. Yuska, J. Am. Chem. Soc. 68, 1681 (1946).

(5) J. I. de Jong and J. de Jonge, Rec. trav. Chim. 72, 139, 207, 213, 1027 (1953).

4. It is proposed that the equilibrium

$$H_2O_2 = 2\ OH$$

and the subsequent decomposition of OH radicals (6) be studied in the shock tube. The OH concentration may be determined spectrophotometrically using the electrodeless discharge through water vapor developed recently at the National Bureau of Standards (7). It might prove possible to use H_2O_2 as a source of OH radicals for other reactions.

(6) C. N. Satterfield and T. W. Stein, J. Phys. Chem. 61, 537 (1957).

(7) H. J. Kostkowski and H. P. Broida, J. Opt. Soc. Am. 46, 246 (1956).

5. Reditzki and Nowinski (8) have found that the catalysis of yeast alcohol dehydrogenase reactions by o-phenanthroline (9) is not effective when the reactants are purified. They interpret this to mean that the original catalysis was due to chelating of traces of heavy metals in the solutions. In view of the large effect involved, it is proposed that before this explanation is accepted some reactions be done in which traces of metal ions are known to be present. Besides more definitely establishing the cause, these experiments would provide data for extrapolation the effect to zero metal concentration.

(8) H. E. Redetzki and W. W Nowinski, Nature 179, 1018 (1957).

(9) B. L. Vallee and F. L. Hoch, Pro. Nat. Acad. Sci. 41, 327 (1955).

6. It is proposed that a spectrophotometric study be made of the colored complexes formed between NO and ferrous ion in acid solution (10). Although known for many years as the basis of the "brown-ring" test for nitrates and nitrites, only one brief examination of the spectra (11)--with no equilibrium data--has been published.

(10) T. Moeller, J. Chem. Ed. 23, 542 (1946).

(11) H. I. Schlesinger and A. Salathe, J. Am. Chem. Soc. 45, 1863 (1923).

7. Preliminary evidence from the coulometric titration of bromate with cuprous copper (12) indicates that the rate of oxidation of cuprous ion by bromine in solution is dependent on the cupric ion concentration. It is proposed that a kinetic study of this effect be made. It may be possible to demonstrate that the catalytic effect of cupric ion is due to the formation of interaction complexes of the type previously found in chloride solutions (13).

(12) G. M. Arcand and E. H. Swift, unpublished experiments.

(13) H. McConnell and N. Davidson, J. Am. Chem. Soc. 72, 3168 (1950).

8. The unstable nitrogen oxide N_2O_2 is described as a chain structure (14) and as a square (15) in the literature. A double labelled isotope exchange reaction between N^{14}-O^{16} and N^{15}-O^{18} is proposed to better determine the structure.

(14) A. L. Smith, W. E. Keller, and H. L. Johnston, J. Chem. Phys. 19, 189 (1951).

(15) W. J. Dulmage, E. A. Meyers, and W. N. Lipscomb, J. Chem. Phys. 19, 1432 (1951).

9. The autooxidation-reduction reaction of ferric thioglycolate in alkaline solution has been assumed to involve a hydroxyl bridged dimer (16). It is proposed that a sulfur bridged dimer is more likely from the final products obtained.

(16) D. L. Leussing and L. Newman, J. Am. Chem. Soc. 78, 552 (1956).

10. It is proposed that another copy of the Journal of Chemical Physics, Volume 19 (1951) be obtained, as the other copy has been missing from the library for several months.